

1  
2  
3  
4  
5  
6  
7  
8  
9  
10  
11  
12  
13  
14  
15  
16  
17  
18  
19  
20

**THEORETICAL ANALYSIS OF ERRORS WHEN ESTIMATING SNOW DISTRIBUTION  
THROUGH POINT MEASUREMENTS**

By

Ernesto Trujillo<sup>1,2</sup> and Michael Lehning<sup>2,1</sup>

1. School of Architecture, Civil and Environmental Engineering, École Polytechnique Fédérale  
de Lausanne, Lausanne, Switzerland

2. WSL Institute for Snow and Avalanche Research SLF, Davos, Switzerland

Corresponding Author:

Ernesto Trujillo  
EPFL ENAC IIE CRYOS, Station 2  
Lausanne, Switzerland, CH-1015  
Email: Ernesto.Trujillo@epfl.ch  
Office: +41 21 693 5938

21        **Abstract**

22        In recent years, marked improvements in our knowledge of the statistical properties of the  
23        spatial distribution of snow properties have been achieved thanks to improvements in measuring  
24        technologies (e.g., LIDAR, TLS, and GPR). Despite of this, objective and quantitative  
25        frameworks for the evaluation of errors and extrapolations in snow measurements have been  
26        lacking. Here, we present a theoretical framework for quantitative evaluations of the uncertainty  
27        of point measurements of snow depth when used to represent the average depth over a profile  
28        section or an area. The error is defined as the expected value of the squared difference between  
29        the real mean of the profile/field and the sample mean from a limited number of measurements.  
30        The model is tested for one and two dimensional survey designs that range from a single  
31        measurement to an increasing number of regularly-spaced measurements. Using high-resolution  
32        (~ 1m) LIDAR snow depths at two locations in Colorado, we show that the sample errors follow  
33        the theoretical behavior. Furthermore, we show how the determination of the spatial location of  
34        the measurements can be reduced to an optimization problem for the case of the predefined  
35        number of measurements, or to the designation of an acceptable uncertainty level to determine  
36        the total number of regularly-spaced measurements required to achieve such error. On this basis,  
37        a series of figures are presented that can be used to aid in the determination of the survey design  
38        under the conditions described, and under the assumption of prior knowledge of the spatial  
39        covariance/correlation properties. With this methodology, better objective survey designs can be  
40        accomplished, tailored to the specific applications for which the measurements are going to be  
41        used. The theoretical framework can be extended to other spatially distributed snow variables  
42        (e.g., SWE) whose statistical properties are comparable to those of snow depth.

43

## 1 Introduction

44 The assessment of uncertainties of snow measurements remains a challenging problem in  
45 snow sciences. Snow cover properties are highly heterogeneous over space and time and the  
46 representativeness of measurements of snow stage variables (e.g., snow depth, snow density, and  
47 snow water equivalent (SWE)) is often overlooked due to difficulties associated with the  
48 assessment of such uncertainties. This has been, at least in part, due to the limited knowledge of  
49 the characteristics of the spatial statistical properties of variables such as snow depth and SWE,  
50 particularly at the small-scales (sub-meter to tens of meters). However, a turning point has been  
51 reached in recent years thanks to improvements in remote sensing of snow (e.g., light detection  
52 and ranging (LiDAR) and Radar technologies), which have allowed significant progress in the  
53 quantitative understanding of the small-scale heterogeneity of snow covers in different  
54 environments, with resolutions and areas of coverage previously unresolved with the standard  
55 methods of measurement (e.g., Trujillo et al., 2007; Trujillo et al., 2009; Mott et al., 2011).

56 Point or local measurements of snow properties will continue to be necessary for purposes  
57 that range from inexpensive evaluation of the amount of snow over a particular area, to  
58 validation of models and remote sensing measurements. Such measurements have a footprint  
59 representative of a very small area surrounding the measurement location (i.e., support,  
60 following the nomenclature proposed by Blöschl (1999)), and the integration of several  
61 measurements is necessary for a better representation of the snow variable in question over a  
62 given area. Because of this, tools for quantitative evaluations of the representativeness and  
63 uncertainty of measurements need to be introduced, and the uncertainty of such measurements  
64 should be more widely discussed in the field of snow sciences.

65 Currently, efforts to assess the reliability and uncertainty of snow measurements have  
66 focused on statistical analyses using point measurements (e.g., Yang and Woo, 1999; Watson et  
67 al., 2006; Rice and Bales, 2010; Lopez-Moreno et al., 2011; Meromy et al., 2013) or  
68 synthetically generated fields in a Monte Carlo framework (e.g., Kronholm and Birkeland, 2007;  
69 Shea and Jamieson, 2010), and comparisons between remotely sensed and ground data (Chang et  
70 al., 2005; Grünewald and Lehning, 2014). These studies have been useful to empirically quantify  
71 uncertainties associated with point measurements; However, these type of approaches do not  
72 provide a quantitative framework for the assessment of uncertainties associated with a particular  
73 sampling design, they do not allow for an optimal sampling strategy (e.g., selecting the number  
74 of points and locations for a desired accuracy level), and they do not take advantage of the  
75 increased knowledge of the characteristics of the heterogeneity of snow cover properties.

76 Another possible approach is one in which the expected error in the estimation of a particular  
77 statistical moment of a field over a defined domain (e.g., areal mean or standard deviation from a  
78 finite number of measurements) is determined on the basis of known statistical properties of the  
79 field in question. Such approach uses geostatistical principles that have been proposed by  
80 Matheron (1955; 1970) and others, and that have been applied in mining geostatistics (Journel  
81 and Huijbregts, 1978), the analysis of uncertainties when measuring precipitation (Rodríguez-  
82 Iturbe and Mejía, 1974), and for a more general analysis of the effects of sampling of random  
83 fields as examples of environmental variables (e.g., Skøien and Blöschl, 2006), among others.  
84 Despite of these examples, there is to the authors' knowledge no attempt of implementing such  
85 type of approach in snow sciences, tailoring the methodology to the particular analysis of  
86 uncertainties when measuring snow variables such as snow depth. Such an implementation  
87 appears to be lacking in numerous studies that use point measurements to represent snow

88 distribution, addressing the spatial extrapolation of such point measurements as the “true” spatial  
89 distribution of snow depth when evaluating the performance of interpolation methodologies,  
90 regressions trees, and hydrological models. These comparisons ignore the intrinsic error incurred  
91 when extrapolating the original point measurements, leaving a proportion of uncertainty that can  
92 be significant unaccounted for. This is the principal motivation of the present study, with the  
93 intention of spreading the use of more objective and quantitative methodologies for error  
94 evaluation in snow sciences. Also, the approach that is presented below can be used for objective  
95 survey design to estimate snow distribution from point measurements. We do not intend to  
96 present our approach as novel in the general geostatistical sense; instead, we present the  
97 derivation with the specific application for snow sciences in mind. However, because of the  
98 general nature of the random fields’ theory that the development is based on, similar  
99 developments can indeed be applied to other environmental variables that can be described as a  
100 random field.

101 On this basis, the error in the estimation of spatial means from point measurements over a  
102 particular domain (e.g., a profile, or an area) can be quantified as the expected value of the  
103 squared difference between the real mean and the sample mean obtained from a limited number  
104 of point measurements. Such an approach, as it will be shown here, uses spatial statistical  
105 properties of snow depth fields in a way that allows for an objective evaluation of the estimation  
106 error for snow depth measurements. The sections below illustrate the use of such methodology  
107 for optimal design of sample strategies in the specific context of snow depth. However, the  
108 methodology can also be implemented for other snow variables such as snow water equivalent,  
109 given that similar geostatistics can be used to characterize their spatial organization.

110

## 2 Background

111 Let  $Z(\mathbf{x})$  denote a random field function of the coordinates  $\mathbf{x}$  in the  $n$ -dimensional space  
 112  $\mathbb{R}^n$ . Bold letters represent a location vector from hereon. In our case, the field can represent e.g.:  
 113 snow depth or snow water equivalent (SWE) at a given time of the year. The mean of the process  
 114 over a domain  $A$  (e.g., a profile section or an area) is defined as:

$$115 \quad \mu_z(A) = \frac{1}{A} \int_A z(\mathbf{x}) d\mathbf{x} \quad (1)$$

116 In practice, the mean is often obtained from the arithmetic average of measurements at a  
 117 finite number of locations,  $N$ , within the domain:

$$118 \quad \bar{Z} = \frac{1}{N} \sum_{i=1}^N z(\mathbf{x}_i) \quad (2)$$

119 The performance of the estimator  $\bar{Z}$  can be evaluated by calculating the expected value of  
 120 the square difference between the estimator  $\bar{Z}$  and the true mean  $\mu_z(A)$

$$121 \quad \sigma_{\bar{Z}}^2(A) = E \left[ \left( \frac{1}{N} \sum_{i=1}^N z(\mathbf{x}_i) - \frac{1}{A} \int_A z(\mathbf{x}) d\mathbf{x} \right)^2 \right] \quad (3)$$

122 For a 1<sup>st</sup> order stationary process (i.e., the mean independent of location; e.g., Cressie (1993),  
 123 section 2; and Journel and Huijbregts (1978), section 2 ), (3) can be expressed as

$$124 \quad \begin{aligned} \sigma_{\bar{Z}}^2(A) &= \frac{1}{N^2} \sum_{i=1}^N VAR[z(\mathbf{x}_i)] + \frac{2}{N^2} \sum_{i=1}^{N-1} \sum_{j=i+1}^N COV[z(\mathbf{x}_i)z(\mathbf{x}_j)] \\ &\quad - \frac{2}{N \cdot A} \sum_{i=1}^N \int_A COV[z(\mathbf{x}_i)z(\mathbf{x}_j)] d\mathbf{x}_j \\ &\quad + \frac{1}{A^2} \int_A \int_A COV[z(\mathbf{x}_i)z(\mathbf{x}_j)] d\mathbf{x}_i d\mathbf{x}_j \end{aligned} \quad (4)$$

125 where  $\text{VAR}[\ ]$  and  $\text{COV}[\ ]$  are the variance and the covariance, respectively. If we further  
 126 assume that the process is second order stationary (e.g., Cressie (1993), section 2; and Journel  
 127 and Huijbregts (1978), section 2), that is, if the mean and the variance are independent of the  
 128 location, and the covariance function depends only on the vector difference  $\mathbf{x}_i - \mathbf{x}_j$ , (3) can be  
 129 expressed as

$$130 \quad \sigma_Z^2(A) = \sigma_p^2 \left[ \begin{aligned} & \frac{1}{N} + \frac{2}{N^2} \sum_{i=1}^{N-1} \sum_{j=i+1}^N \text{CORR}[\mathbf{x}_i - \mathbf{x}_j] \\ & - \frac{2}{NA} \sum_{i=1}^N \int_A \text{CORR}[\mathbf{x}_i - \mathbf{x}_j] d\mathbf{x}_j \\ & + \frac{1}{A^2} \int_A \int_A \text{CORR}[\mathbf{x}_i - \mathbf{x}_j] d\mathbf{x}_i d\mathbf{x}_j \end{aligned} \right] \quad (5)$$

131 where  $\text{CORR}[\ ]$  is the correlation function, and  $\sigma_p^2$  is the variance of the point process.

132 The first two terms in (5) are the total sum of the covariances (or correlation as  $\sigma_p^2$  has been  
 133 factored out) between all point locations  $i = 1, \dots, N$  (e.g., measurement locations). The first of  
 134 the two terms is only a function of the number of points, while the second is a function of the  
 135 number of points,  $N$ , and the correlations between the locations. Such correlations are themselves  
 136 a function of the separation vectors (both in magnitude and direction), and the parameters of the  
 137 correlation function. These two terms are independent of the size of the area  $A$ , and can be  
 138 thought of as the portion of the error caused by the correlation between the point processes at the  
 139 locations  $i = 1, \dots, N$  (e.g., measurement locations). Term 3 accounts for the correlation between  
 140 the measurement locations and the continuous process over the domain  $A$ . This term can be seen  
 141 as a negative contribution to the total error assuming that the sum of the integrals is positive. The  
 142 term is a function of the number of points,  $N$ , the domain area,  $A$ , the location of the points and

143 the correlation structure, characterized using the parameters of the correlation function. Lastly,  
144 term 4 is the contribution to the error caused by the intrinsic correlation structure of the  
145 continuous process over the domain. This term is a function of the domain (e.g., size and shape  
146 of  $A$ ) and the correlation structure (e.g., parameters of the correlation function).

### 147 **3 Data**

148 For the analyses and tests of the methodology presented here, Light Detection and Ranging  
149 (LIDAR) snow depths obtained as part of the NASA's Cold Land Processes Experiment (CLPX)  
150 will be used (Cline et al., 2009). The dataset consists of spatially distributed snow depths for 1-  
151 km x 1-km areas (Intensive Study Areas - ISAs) in the Colorado Rocky Mountains close to  
152 maximum snow accumulation in April, 2003. The data were processed from snow-on (8-9 April,  
153 2013) and snow-off (18-19 September, 2013) LIDAR elevation returns with an average  
154 horizontal spacing of 1.5 m and vertical tolerance of 0.05 m. The final CLPX snow depth  
155 contour product (0.10 m vertical spacing) was generated from these returns. This product was  
156 used to generate gridded snow depth surfaces with 1024x1024 elements over the ISAs, for a grid  
157 resolution of 0.977 m. For this study two areas will be used: the Fraser – St Louis Creek ISA  
158 (FS) and the Rabbit Ears – Walton Creek ISA (RW) (Figure 1). The FS ISA is covered by a  
159 moderate density coniferous (lodgepole pine) forest on a flat aspect with low relief. The RW ISA  
160 is characterized by a broad meadow interspersed with small, dense stands of coniferous forest  
161 and with low rolling topography. The snow depth distributions in these ISAs show differences  
162 that are relevant for the analysis of the methodology introduced here. At the FS ISA, the snow  
163 depth distribution is relatively isotropic (Figure 1b), with short spatial correlation memory and  
164 little variations in the spatial scaling properties (i.e., power-spectral exponents and scaling  
165 breaks) with direction (Trujillo et al., 2007). On the other hand, the spatial distribution of snow



166 depth in the RW ISA is more anisotropic (Figure 1c), with longer spatial correlation memory  
167 along a principal direction aligned with the predominant wind direction versus shorter memory  
168 along the perpendicular direction, and with variations in the power-spectral exponents and  
169 scaling breaks according to the predominant wind directions (Trujillo et al., 2007).

#### 170 **4 One-dimensional process**

171 The spatial representation of the snow cover requires a basic assumption on the scale or  
172 resolution at which a field or profile is going to be represented. This relies on the spatial support  
173 of the measurements. For the case of snow depths, point measurements from local surveys using  
174 a snow depth probe are frequently used for this representation. Generally, there are additional  
175 sources of uncertainty associated with these types of measurements, such as the accuracy of the  
176 position of the measurement in space or deviations in the vertical angle of penetration of the  
177 probe through the snow pack. These uncertainties are additional to any of the uncertainties  
178 estimated using the methodology discussed here.

179 The one-dimensional case provides a good opportunity to illustrate the limitations of point  
180 measurements. Consider the case of a snow depth profile that is measured using a snow depth  
181 probe at a regular spacing “d”. Each of these point measurements is meant to represent the mean  
182 snow depth over a particular distance surrounding the measurement, and the question is: over  
183 what distance is such assumption valid? In this case, the intrinsic assumption is that the  
184 measurement is representative over the distance “d”, but at this point the validity of such  
185 assumption is not proven.

186 The answer to this question is conditioned to how variable the profile is and over what  
187 distances. To look at this, let us look at two snow depth profiles, one in a forested environment

188 (FS) and another in an open environment (RW) in the Colorado Rocky Mountains (Figure 2a and  
189 Figure 3a, respectively). The variability in the profiles is markedly different, with variations over  
190 shorter distances in the forested area, and a smoother profile in the open and wind influenced  
191 environment. This is reflected in the spatial correlation structure of these snow depth profiles,  
192 with stronger correlations over longer distances in open and wind-influenced environments with  
193 respect to that in forested environments (Trujillo et al., 2007; Trujillo et al., 2009). These  
194 differences should be considered when selecting the sampling frequency required to capture the  
195 variability and accurately represent the mean conditions within a particular sampling spacing.  
196 This is illustrated by comparing the mean snow depth for a particular resolution to the point  
197 value at the center of the interval (Figure 2b in a forested environment and Figure 3b in an open  
198 and wind-influenced environment). In the Figures, average versus point values at several  
199 sampling intervals are compared for normalized profiles ( $\mu = 0$ ,  $\sigma = 1$ ) separated every 30 m in  
200 both the  $x$  (east) and  $y$  (north) directions and for an area of 500 m by 500 m. The 30-m separation  
201 between profiles is chosen to reduce the spatial correlation between them. Firstly, the resulting  
202 comparison shows that the point values generally overestimate the variability in mean snow  
203 depths if we replace the mean snow depth distribution by its point sample. To clarify this, let us  
204 consider here two snow depth profiles, one with the snow depths at the nominal scale ( $\sim 1$  m),  
205 and a second one with a moving average (MA) of the first one with an averaging window equal  
206 to the sampling spacing. Ultimately, the variance/standard deviation of the first profile ( $\sim 1$  m) is  
207 larger than that of the MA, with a distribution that reflects these differences. The samples drawn  
208 from the first profile will reflect a larger variance than that of the samples from the MA profile as  
209 they are drawn from these distributions, and this is what is reflected in Figure 2 and Figure 3.  
210 The degree of overestimation can be quantified through the slope of the regression line (in red in

211 Figure 2b and Figure 3b). In the forested environment (Figure 2b), the slopes range between 0.8  
212 and 0.13, with decreasing slopes with increasing spacing. These slopes indicate that, on average,  
213 the mean values are 0.8 times the point values for the 5 m spacing and 0.1 times the point values  
214 for the 100 m spacing. In the open and wind-dominated environment, the slopes are higher and  
215 range between 0.97 and 0.23 from 5 m spacing and 100 m spacing, respectively. A clear  
216 difference emerges: forested environments require shorter separation between single  
217 measurements if the snow depth profile is to be accurately captured by the measurements. The  
218 variability within the size of the interval determines the degree of uncertainty associated with the  
219 point measurements, as the sub-interval variability is related to the degree of overestimation of  
220 the mean value within the interval. Secondly, the differences between average and point values  
221 for each spacing distance are generally more scattered in the forested environment than in the  
222 open environment, and in both environments the degree of scattering increases with spacing  
223 (Figure 2c and Figure 3c). However, it is important to note here that we are comparing  
224 normalized profiles ( $\mu = 0$ ,  $\sigma = 1$ ), allowing us to focus on the rescaled spatial variations. What is  
225 highlighted is the relevance of the spatial structure of the profile rather than the absolute  
226 variance. This spatial structure can be quantified by, for example, the spatial  
227 covariance/correlation function.

228 Additionally to the differences in the correlation structure, there are also differences in the  
229 absolute variability in snow depth in these environments (Figure 4). As opposed to the  
230 normalized snow depth discussed above, the subinterval standard deviation as a function of  
231 interval size along the profiles is higher in the open and wind-influenced environment at RW  
232 versus the forested environment at FS (Figure 4a). Mean standard deviation values in the open  
233 environment are twice as large as those at the forested environment towards the larger interval

234 sizes (~100 m). The standard deviation increases with interval size in both environments, with  
235 the steepest increase at the lower interval sizes. Furthermore, the standard deviation tends to  
236 stabilize more rapidly in the forested environments, with an increase of only 1.8 cm between 30  
237 m and 100 m. On the other hand, the standard deviation continues to increase in the open  
238 environment at RW, with less of an asymptotical behavior for the scales analyzed.  
239 Complementary, the shaded areas (25% to 75% quantiles) give an idea of the variability of  
240 standard deviation values, with a much wider range in RW versus FS, and an increase in the  
241 range between quantiles with interval size in RW.

242 Consistent with the standard deviation, the sub-interval mean range (range defined as the  
243 difference between the maximum and minimum snow depths within an interval) increases with  
244 interval size in both FS and RW (Figure 4b). However, the mean range is larger in the open  
245 environment at RW and the rate of increase with interval size is also steeper. Similarly, the  
246 shaded areas indicate wider distribution of range values in the open environment at RW, while  
247 relatively uniformly distributed around the mean across interval sizes in the forested environment  
248 at FS. The results in Figure 2-Figure 4 illustrate this contrasting behavior between the snow  
249 covers in these environments and their influence on measurement strategies: that is, the forested  
250 environments requires shorter separation between measurements for accurate representation of  
251 the snow cover, however, in the wind-influence and open environment, the subinterval  
252 variability is higher indicating wider variations around any sampled measurement within the  
253 interval.

254 Ultimately, the number and distance between measurements and the specific arrangement of  
255 the measurements are all conditioned to what the measurements are needed for. Hydrologic  
256 applications may not require a highly detail representation of a snow depth profile (or a field),

257 and representing the average conditions over a given distance (or area) is sufficient, but small-  
 258 scale process-based studies may require a more detailed characterization over shorter distances  
 259 (or smaller areas). This implies that the decision depends on the particular use that the  
 260 measurements will support. In the following sections, the equations presented in the Background  
 261 (section 2) will be applied to evaluate the uncertainty associated with multiple measurement  
 262 designs for profiles and fields of snow depth.

#### 263 4.1 Case 1: Single measurement along a profile section

264 Equation (2) can be used to evaluate the uncertainty of a single measurement along a profile  
 265 section of length  $L$ . For this case, as well as for the following cases in this article, an exponential  
 266 covariance with a decay exponent  $\nu$  ( $\nu > 0$ ) will be assumed:

$$267 \quad COV(\mathbf{h}, \sigma, \nu) = \sigma^2 \exp(-\nu \|\mathbf{h}\|) \quad \text{for } \sigma^2 > 0, \text{ and } \nu > 0 \quad (6)$$

268 where  $\sigma^2$  is the variance, and  $\|\mathbf{h}\|$  is the length of the vector  $\mathbf{h}$ . For this one-dimensional case  
 269 and combining (6) and (5), the following expression is obtained:

$$270 \quad \sigma_z^2(x, L, \nu) / \sigma_p^2 = 1 - \frac{2}{Lv} \left[ 2 - \exp(-\nu x) - \exp(-\nu \cdot [L - x]) \right] + \frac{1}{L^2 \nu} \left[ 2L + \frac{2}{\nu} \exp(-\nu L) - \frac{2}{\nu} \right]$$

271 (7)

272 where  $x$  is the distance from one extreme of the section to the location of the measurement  
 273 (Figure 5a). The normalized squared error  $\sigma_z^2(x, L, \nu) / \sigma_p^2$  is minimized at  $x$  equal to half of the  
 274 section length,  $L/2$ , regardless of  $\nu$ . The existence of a correlation in the profile leads to this  
 275 solution, as the middle location contains more information about its surroundings. Also, this  
 276 solution is different from the solution for an uncorrelated profile (e.g., white noise), for which

277 the squared error would be equal to the variance, independent of the location of the  
278 measurement.

279 The results here are confirmed with an analysis of LIDAR snow depths profiles in FS and  
280 RW (Figure 6). The analysis consists of calculating the difference between the mean and the  
281 point value for sections of a given length (varied between 10 m – 50 m) and for  $x$  (Figure 5a)  
282 between 0 and  $L$  along the profile sections. Each sample section of length  $L$  will provide a single  
283 difference for each of the  $x$  values. These sample differences are then used to calculate the mean  
284 normalized squared error for each  $x$ , and the same is repeated for each section length  $L$ . The  
285 results indicate that the real snow depth profiles behave as predicted by the model of the error,  
286 with a minimum error at  $x$  equal to half of the section length. Another difference highlighted by  
287 these results is the difference between the sample errors in the forested environment (FS) versus  
288 the open environment (RW) for the larger interval sizes (e.g., 50 m). The sampled normalized  
289 squared error in the forested environment shows only a mild decrease in the square error to  
290 around 0.7-0.8 towards the inside of the section length. However, this decrease is achieved for  
291 the measurement along most of the interval length with the exception of the extremes. This can  
292 be explained by the relationship between the spatial memory of snow depth (e.g., the correlation  
293 function) and the section length. Densely forested environments exhibit correlation lengths that  
294 are shorter than those in open and wind influenced environments (e.g., Trujillo et al., 2007;  
295 Trujillo et al., 2009). As the section length increases beyond such correlation lengths, a  
296 measurement location towards the middle of the interval contains less information of the  
297 surrounding snow depths in a forested environment (e.g., FS) versus an open and wind  
298 influenced environment (e.g., RW). This is observed in Figure 6c versus Figure 6f, with the  
299 results in RW showing a more clear minimum towards the center of the profile section. The

300 results also show a poorer performance of the model in RW versus FS, as the exponential  
301 correlation model has a poorer fit in RW at the shorter-lag range; However, model performance  
302 is improved for longer section lengths (e.g., Figure 6c and f)

303 Model and sampled results thus support that the measurement location can be fixed in the  
304 middle of the interval, and the normalized squared error can then be described as a function of  
305 both, the exponential decay exponent,  $\nu$ , and the length of the section,  $L$  (Figure 7a). The  
306 normalized squared error increases with interval length, with a steeper increase for larger  
307 exponential decay exponents, for which the squared error approaches that of an uncorrelated  
308 field more rapidly. The theoretical model is tested on the snow depth fields at FS and RW. The  
309 test consists of calculating the sampled normalized squared error as the average of all squared-  
310 differences between the mid-section snow depth and the mean from all LIDAR grid-points  
311 within each interval of length  $L$ . This is done for profiles separated every 30 m, similar to the  
312 analysis above, and for profiles along the  $x$  and  $y$  directions. The theoretical normalized squared  
313 error is estimated from (7) using the exponential decay exponent from the model fitted to the  
314 sampled correlation function. The results show that the theoretical model reproduces the sampled  
315 squared error remarkably well, even reproducing the anisotropic properties of the correlograms,  
316 represented by the different exponents of the exponential model along  $x$  and  $y$  directions (Figure  
317 7b and c). The model also reproduces the different behavior of the squared error between both  
318 fields (i.e., FS and RW), showing that the normalized squared error increases more rapidly and is  
319 larger in the forested environment (Figure 7b) versus the open environment (Figure 7c).  
320 However, it should be noted here that as the error is normalized and as the variance of the field in  
321 the open environment is larger (Figure 4a), the absolute squared error could reach higher values  
322 in the open environment (RW). In this regard, one feature to discuss here is the assumption that

323 the point variance of snow depth in these environments has been estimated as the spatial variance  
 324 over the entire study area, as it is generally practiced in time series analysis and geostatistics. In  
 325 practice, this is the only possible approach because there is limited information to estimate the  
 326 point variance from multiple realizations of the process at each spatial location, as inter- and  
 327 intra- annual snow depth fields are not available, not only for these areas, but for almost any area  
 328 where this methodology may be applied.

#### 329 4.2 Case 2: Three measurements along a profile section

330 From (5) it is also evident that increasing the number of measurements will reduce the  
 331 squared error. In the case of three measurements separated by a distance ‘ $a$ ’, with the middle  
 332 measurement centered in the section of length  $L$  (Figure 5b), and for an exponential covariance  
 333 function with parameter  $\nu$ , (5) leads to the following expression for this particular case:

$$\begin{aligned}
 \sigma_z^2(a, L, \nu) / \sigma_p^2 &= \frac{1}{3} + \frac{2}{9} [2 \exp(-\nu a) - \exp(-2\nu a)] \\
 334 \quad &- \frac{4}{3L\nu} \left[ 3 - \exp\left(-\frac{\nu L}{2}\right) (1 + \exp(-\nu a) + \exp(\nu a)) \right] \\
 &+ \frac{1}{L^2\nu} \left[ 2L + \frac{2}{\nu} \exp(-\nu L) - \frac{2}{\nu} \right]
 \end{aligned} \tag{8}$$

335 Equation (8) can be minimized to determine the optimal separation distance between points,  
 336  $a$ , as a function of  $L$  and  $\nu$ :

$$337 \quad a_{optimal} = -\frac{1}{\nu} \ln(t) \tag{9}$$

338 where

$$339 \quad t = \frac{B + \sqrt{B^2 - 4AB}}{2A}$$



340 
$$A = \frac{4\nu}{9}$$

341 and 
$$B = -\frac{4}{3L} \exp\left(-\frac{\nu L}{2}\right)$$

342 The combination of (8) and (9) can be used to determine the normalized squared error,  
343  $\sigma_z^2/\sigma_p^2$ , and the optimal distance,  $a_{optimal}$ , for the measurement pattern in Figure 5b. The model  
344 predicts that the normalized squared error is minimized at an intermediate location between 0  
345 and  $L/2$  (black lines in Figure 8a and b). The results show an increase in the error with interval  
346 size,  $L$ , as well as little sensitivity of  $a_{optimal}$  to  $\nu$ . This latter feature can be seen as an advantage  
347 since small biases in the estimation of  $\nu$  will not result in significant biases in the estimation of  
348  $a_{optimal}$ . One could almost assume a value of  $a_{optimal}$  without prior knowledge of the exponential  
349 decay exponent, selecting  $a_{optimal}$  within the range of values indicated by the model for a range of  
350 possible exponential decay exponents. Note that  $a_{optimal}$  is located close to the 60% distance from  
351 the center towards the outer boundary of the profile section for all section lengths (Figure 8a and  
352 b). On the other hand, the measurement error displays a higher sensitivity to  $\nu$  around  $a_{optimal}$ ,  
353 indicating that biases in the estimation of  $\nu$  would have a more noticeable effect on the  
354 estimation of the measurement error. This is further clarified in Figure 8c, in which the  
355 normalized error (not squared) and  $a_{optimal}$  can be obtained for corresponding profile section  
356 lengths ( $L$ ) and exponential decay exponents ( $\nu$ ) based on the isolines shown. For example, for a  
357 profile section of 30 m, and an exponential decay exponent of  $0.2 \text{ m}^{-1}$ , the normalized error is  
358 0.32 and  $a_{optimal}$  is 9.63 m (see intersect of the two isolines in Figure 8c). The normalized error in  
359 Figure 8c is not squared, highlighting the sensitivity of the measurement error to  $\nu$ , which

360 represents the degree of spatial correlation of the profile in this case (e.g., lower values indicate  
361 stronger spatial memory/correlation, hence lower measurement errors).

362 The performance of the model is tested against the normalized squared error obtained from  
363 the same snow depth profiles in FS and RW. The test consists of estimating the normalized  
364 squared error for profiles sections of length between 10 m and 80 m, with  $a$  being varied between  
365 0 and  $L/2$  (Figure 9). For each value of  $a$ , the normalized squared error is estimated based on the  
366 means obtained using the three snow depth samples for each section. All squared differences are  
367 then averaged to obtain the values presented in the Figure. Sampled and modeled errors follow  
368 the same trend across all  $a$  values and for the different  $L$  values in Figure 9. The minimum error  
369 is also reproduced by the model proving the applicability of the model for estimating the optimal  
370 separation between measurements. The model does perform better in the forested environment of  
371 FS versus RW, particularly for lower  $a$  values. This can be justified as the exponential  
372 covariance model displays a better fit in FS over RW, particularly over the lower range of lag  
373 values. Also, note that both the modeled and sampled normalized squared errors are lower for the  
374 snow depth profiles at RW because of the longer spatial memory of the snow depth distribution  
375 in this environment (higher spatial correlations) when compared to that in FS.

### 376 **4.3 Case 3: $N$ measurements along a profile section**

377 As stated above, the measurement error can be reduced by increasing the number of  
378 measurements taken over a given section of length  $L$ . Let us focus on the case of stratified  
379 sampling where  $N$  regularly spaced measurements are taken over the interval (Figure 5c), and to  
380 quantify this reduction we can use (5) and the exponential covariance model. Equation (5) can  
381 then be reduced to:

$$\begin{aligned}
\sigma_z^2(N, L, \nu) / \sigma_p^2 &= \frac{1}{N} + \frac{2}{N^2} \sum_{k=1}^{N-1} k \exp\left(-\nu \left[ L - kL/N \right] \right) \\
&- \frac{4}{L\nu} \left[ 1 - \frac{1}{N} \sum_{k=1}^N \exp\left(-\nu \frac{L}{N} \left[ N - k + \frac{1}{2} \right] \right) \right] \\
&- \frac{2}{L^2 \nu^2} [1 - L\nu - \exp(-\nu L)]
\end{aligned} \tag{10}$$

383 The normalized squared error ( $\sigma_z^2 / \sigma_p^2$ ) obtained with (10) for profiles sections of lengths  
384 between 10 and 80 shows a steep decrease with  $N$  (Figure 10), with a steeper decrease for higher  
385 exponential decay exponents. For the longer profile sections (e.g., 80, Figure 10d), little  
386 reductions are achieved in the squared error beyond only a few measurements (e.g.,  $N = 16$ ).  
387 Equation (10) and the results in Figure 10 can be used to determine the number of measurements  
388 necessary to achieve a desired accuracy level. One could, for example, design a survey to sample  
389 a snow depth profile with a mean value every 10 m. The number of measurements required to  
390 achieve a desired level of accuracy can be obtained from Figure 10a, based on previous  
391 knowledge of the sample estimate of the exponential decay exponent. This can be achieved  
392 thanks to the intra-annual and inter-annual persistence of the spatial patterns, and hence, the  
393 spatial statistical properties of snow depth fields in mountain environments, as shown in previous  
394 studies using both manual surveys and LIDAR measurements (e.g., Deems et al., 2008; Sturm  
395 and Wagner, 2010; Schirmer et al., 2011; Melvold and Skaugen, 2013; Helfrich et al., 2014). A  
396 detailed spatial survey (e.g., dense manual measurements or TLS), sampling different portions of  
397 an area can be used to determine the covariance/correlation characteristics of the snow depth  
398 distribution, with which the model for the error can be applied. An a priori estimate of the  
399 exponential decay exponent may also be possible and will be tested in future applications of the  
400 framework, given the relative insensitivity of the error with respect to  $\nu$ .

401 Following the method described in the previous section, we test the performance of the  
402 model against the normalized squared error obtained from the same snow depth profiles in FS  
403 and RW. In this case, the sampled squared error is estimated based on the  $N$  regularly-spaced  
404 measurements distributed along the profile sections of length  $L$ . As the snow depth fields are  
405 gridded at  $\sim 1$ -m resolution, the location of the measurements is approximated to the closest  
406 coordinate in the profile section following the pattern in Figure 5c. Once again, sampled and  
407 modeled errors follow closely the same trend for the different  $L$  values in both FS and RW  
408 (Figure 11). The error decreases with  $N$ , with a rapid decay at the lower  $N$  values, illustrating that  
409 the error can be drastically reduced by simply increasing the number of measurements by a small  
410 amount. The normalized squared error across all  $N$  values is lower for RW than for FS,  
411 consistent with the higher spatial correlations observed in the snow depth fields of RW versus  
412 FS. Once again, there are some differences between the sampled and modeled normalized  
413 squared error in RW for the shorter profile lengths and for small  $N$  values: a consequence of the  
414 poorer fit of the exponential model for the shorter lag range in RW. However, the model is still  
415 able to reproduce the error in both fields, and the applicability of the model is illustrated even  
416 when the fit of the correlation model can be improved.

## 417 **5 Two-dimensional process**

418 Similar to the one-dimensional process, equation (5) can be formulated to calculate the  
419 squared error in the two-dimensional space. To exemplify this, we apply the methodology to an  
420 isotropic process over the  $x$ - $y$  plane for three cases in a square area: (a) one single measurement  
421 in the center of the area, (b) five measurements radiating out from the center (Figure 12a), and  
422 (c)  $N$  by  $N$  measurements regularly spaced in the  $x$  and  $y$  directions (Figure 12b).

423 For the isotropic case, the covariance/correlation function is only dependent on the  
 424 magnitude of the lag vector,

$$425 \quad h_{i,j} = |\mathbf{x}_i - \mathbf{x}_j| \quad (11)$$

426

427 and, consequently, the error is represented by,

$$428 \quad \sigma_{\bar{z}}^2(A) = \sigma_p^2 \left[ \begin{aligned} & \frac{1}{N} + \frac{2}{N^2} \sum_{i=1}^{N-1} \sum_{j=i+1}^N CORR[h_{i,j}] \\ & - \frac{2}{NA} \sum_{i=1}^N \int_A CORR[h_{i,j}] d\mathbf{x}_j \\ & + \frac{1}{A^2} \int_A \int_A CORR[h_{i,j}] d\mathbf{x}_i d\mathbf{x}_j \end{aligned} \right] \quad (12)$$

429

430 The exponential correlation function for the isotropic case takes the following form:

$$431 \quad CORR(h,v) = \exp(-vh) \quad (13)$$

432 where  $h$  is the magnitude of the lag vector. Replacing into the expression for  $\sigma_{\bar{z}}^2$ , we obtain,

$$433 \quad \sigma_{\bar{z}}^2 = \sigma_p^2 \left[ \begin{aligned} & \frac{1}{N} + \frac{2}{N^2} \sum_{i=1}^{N-1} \sum_{j=i+1}^N \exp(-v|\mathbf{x}_i - \mathbf{x}_j|) \\ & - \frac{2}{NA} \sum_{i=1}^N \int_A \exp(-v|\mathbf{x}_i - \mathbf{x}_j|) d\mathbf{x}_j \\ & + \frac{1}{A^2} \int_A \int_A \exp(-v|\mathbf{x}_i - \mathbf{x}_j|) d\mathbf{x}_j d\mathbf{x}_i \end{aligned} \right] \quad (14)$$

434 For the case of a rectangular area of side dimension  $L_x$  and  $L_y$  in the corresponding  $x$  and  $y$   
 435 directions, the equation becomes,

$$\sigma_{\bar{Z}}^2 = \sigma_p^2 \left[ \begin{aligned} & \frac{1}{N} + \frac{2}{N^2} \sum_{i=1}^{N-1} \sum_{j=i+1}^N \exp\left(-\nu\left((x_i - x_j)^2 + (y_i - y_j)^2\right)^{1/2}\right) \\ & - \frac{2}{NA} \sum_{i=1}^N \int_0^{L_y} \int_0^{L_x} \exp\left(-\nu\left((x_i - x)^2 + (y_i - y)^2\right)^{1/2}\right) dx dy \\ & + \frac{1}{A^2} \int_0^{L_y} \int_0^{L_x} \int_0^{L_y} \int_0^{L_x} \exp\left(-\nu\left((x' - x)^2 + (y' - y)^2\right)^{1/2}\right) dx dy dx' dy' \end{aligned} \right] \quad (15)$$

437 The limits of the integrals can be changed depending on the desired location of the origin. In  
438 this case, the origin is located at the lower-left corner.

439 As discussed earlier, the first term is only a function of  $N$ , such that the base error is the  
440 variance of the point process divided by the number of points. The second term is a function of  
441  $N$ , the location of the points, and the decay rate  $\nu$ . The third term is a function of  $N$ ,  $A$ , the  
442 location of the points, and the decay rate  $\nu$ . The fourth term is a function of  $A$  and  $\nu$ , but is  
443 independent of the location of the points and  $N$  (i.e., independent of the survey design, and only a  
444 function of the correlation structure of the continuous process).

### 445 5.1 Case 1: Single measurement in the center of the area

446 In this case, we focus on a single measurement in the middle of a square area of side  
447 dimension  $L$ . Numerical solution of (15) shows that the normalized squared error increases  
448 rapidly with  $L$ , with a steeper increase for higher exponential decay exponents (Figure 13a),  
449 which approach a normalized squared error of 1 for  $L$  values less than 10 (e.g.,  $1 \leq \nu \leq 5$ ). The  
450 theoretical results in Figure 13a can be used to determine the discrepancy between a single  
451 measurement in the middle of an area and the areal mean for a second order stationary and  
452 anisotropic process with an exponential covariance/correlation function. Comparison of the  
453 modeled and sampled normalized square errors for the FS snow depth field indicate very good  
454 agreement between modeled and sample errors (Figure 13b). The sample error is estimated

455 following the same procedure explained for the one-dimensional cases, although in the two-  
456 dimensional space. Both sampled and modeled errors show the same behavior across  $L$  values  
457 between 1 m and 100 m, although the scatter in the sampled error increases for larger  $L$  values.  
458 This can be explained by the smaller number of samples to estimate the mean normalized  
459 squared error and the fact that the correlation structure decays rapidly and a single sample  
460 becomes less correlated to the surrounding area for these larger areas. The model introduced here  
461 can then be used to assess the representativeness of a single measurement over an area  
462 objectively and accurately, and it can be extended for other covariance/correlation functions as  
463 needed.

## 464 **5.2 Case 2: Five measurements radiating out from the center of the area**

465 The case five measurements radiating out from the center (Figure 12a), with a point in the  
466 middle of the area and four points separated by a distance  $a$  from the center leads to a similar  
467 optimization problem as illustrated in case 2 of the one-dimensional examples (section 4.2). In  
468 the two-dimensional case, (15) does not have an explicit solution for  $a$ , and numerical  
469 implementation is required. The equation can be solved by simply replacing the point  
470 coordinates and the correlation function parameters. Following this approach, the normalized  
471 squared error can be obtained for areas of varying sizes (Figure 14). Similar to the one-  
472 dimensional example (case 2, section 4.2),  $\sigma_z^2/\sigma_p^2$  decreases with  $a$ , reaching a minimum at an  
473 intermediate distance from the middle point outwards. The decay in  $\sigma_z^2/\sigma_p^2$  is more rapid for  
474 the least correlated processes (i.e., higher decay exponents) reaching a value close to the base  
475 normalized square error that is a function of the number of points (i.e.,  $1/N = 1/5$  in this case). An  
476 extended analysis of the effect of each of the terms in the equation is included in the

477 Supplementary Information. The error, as shown in Figure 14, is minimized as a consequence of  
478 two balancing terms that lead to this intermediate solution. The optimal solution is a balance  
479 between reducing the correlation between the individual measurements (e.g., increasing the  
480 separation between the location of the measurements) but increasing the correlation between the  
481 measurements and the surrounding area (e.g., locating the measurements closer to the middle of  
482 the area). These two competing effects lead to an optimization problem based on the location of  
483 the point measurements. For the least correlated processes, the error behaves closer to the  
484 behavior of an uncorrelated field once the measurements become effectively decorrelated (e.g.,  $a$   
485  $> 1$  in Figure 14b for  $\nu = 5$ ). Figure 14 exemplifies how (15) can be used to determine the  
486 optimal measurement location for areas of different sizes, and to determine the associated error  
487 with configurations other than the optimal.

488 The performance of the model is tested against the normalized squared error obtained from  
489 the snow depth field in FS. The test consists of estimating the normalized squared error for  
490 square areas of side dimension ( $L$ ) between 10 m and 79 m, with  $a$  being varied between 0 and  
491  $L/2$  (Figure 15). For each value of  $a$ , the normalized squared error is estimated based on the  
492 means obtained using the five snow depth samples for each section. All squared differences are  
493 then averaged to obtain the values presented in the figure. Once again, the sampled and modeled  
494 errors follow the same trend across all  $a$  values and for the different  $L$  values. The minimum  
495 error and  $a_{optimal}$  are also reproduced closely by the model, and as the area size increases, the  
496 sampled and modeled error approach the error for an uncorrelated field at larger separations (i.e.,  
497 0.2). These results illustrate that the performance of the model in the two-dimensional space is  
498 remarkable, similar to what was observed in the one-dimensional case.



### 499 5.3 Case 3: $N$ by $N$ measurements regularly spaced in the $x$ and $y$ directions

500 Similarly to the one-dimensional case, the two-dimensional case of  $N$  by  $N$  regularly spaced  
501 measurements (Figure 12b) leads to a decreasing normalized squared error with  $N$  (Figure 16).  
502 There is a sharp decrease in the error with just increasing the number of measurements in the  
503 lower range of  $N$ . The analysis illustrates that stratified sampling, as the one shown here, is an  
504 excellent approach to minimizing the error. For example, for the area of 10 by 10, increasing  $N$   
505 to 4 ( $N^2 = 16$ ) reduces the normalized squared error to less than 0.05. It is also worth noting here  
506 that for this two-dimensional case, the error is less sensitive to the value of the exponential decay  
507 exponent ( $\nu$ ) for the higher  $N$  values as the mean is accurately captured regardless of the  
508 correlation of the field. Beyond a certain number of measurements regularly distributed in the  
509 area, the measurements gather enough information such that there are only very minor  
510 improvements with the addition of new measurements, regardless of the exponent value. Figure  
511 16 serves as an example of how the methodology can be used for objective selection of the  
512 number of measurements necessary to achieve a desired accuracy level using prior knowledge of  
513 the spatial covariance function.

514 The performance of the model is tested again for square areas of side dimension ( $L$ ) between  
515 10 m and 79 m using the snow depth field in FS, and for an increasing number of rows/columns  
516 of measurements leading to a total number of measurements of  $N^2$  (Figure 17). The results  
517 illustrate again the accurate performance of the theoretical model, with sampled and model errors  
518 following closely the same squared errors. Both sampled and modeled errors increase as the size  
519 of the area increases, as expected. These results complete the model performance tests for the  
520 two-dimensional isotropic case.

521

## 6 Summary and Conclusions

522 A methodology for an objective evaluation of the error in capturing mean snow depths from  
523 point measurements is presented based on the expected value of the squared difference between  
524 the real average snow depth and the mean of a finite number of snow depth samples within a  
525 defined domain (e.g., a profile section or an area). The model can be used for assisting the design  
526 of survey strategies such that the error is minimized in the case of a limited and predetermined  
527 number of measurements, or such that the desired number of measurements is determined based  
528 on a predefined acceptable uncertainty level. The model is applied to one- and two-dimensional  
529 survey examples using LIDAR snow depths collected in the Colorado Rockies. The results  
530 confirm that the model is capable of reproducing the estimation error of the mean from a finite  
531 number of samples for real snow depth fields.

532 Here, we should highlight some of the implications of the assumptions made in the model. In  
533 simplified terms, the second-order stationarity assumption implies that the mean and the variance  
534 of the process/variable (e.g., snow depth) are independent of the spatial location, and that the  
535 covariance is dependent only on the separation vector (i.e., lag). Although these assumptions  
536 may not be as adequate over larger scales (e.g., greater than 100 m), at smaller scales the  
537 assumption in the context of the model application to snow depth should be valid. We present  
538 these examples to show how the error can be quantified with good accuracy around such smaller  
539 scales. Application of such types of approaches at larger scales will require additional  
540 evaluations with particular attention as to what the specific demands of the application are. Also,  
541 the methodology as presented here is not suitable for discontinuous snow covers if both snow-  
542 covered and snow-free areas are considered in the error estimation. This case has not been  
543 considered in the development here.

544 Implementation of the model in practice requires prior assumption of a  
545 correlation/covariance model and estimates of the parameters of this model (e.g., the decay  
546 exponent for the exponential case). In the examples here we use LIDAR data for the parameter  
547 estimation, which we have done to illustrate the applicability of the model and its ability to  
548 estimate the error using real snow depth data. Snow distribution in mountain environments has  
549 been shown to be consistent intra- and inter-annually because the controlling processes are  
550 relatively consistent during the season and from season to season. Such consistency suggests that  
551 the correlation/covariance model should also be consistent, as well as the parameters of the  
552 model. These parameters can be estimated via a dense survey either manually or with TLS of one  
553 or more small plots of a size similar to the size that is aimed to be represented. These surveys  
554 would not necessarily have to be repeated as the parameters and covariance models should be  
555 preserved. Detailed surveys can be conducted under different conditions to characterize the range  
556 of the correlation models and parameters (e.g., after a snow storm, or close to peak  
557 accumulation). Also here, we should point out that although we show results for a wide range of  
558 the exponential decay exponent values, we are finding that most of the values that we have  
559 observed are in the lower range of those presented (e.g.,  $0.1-0.2 \text{ m}^{-1}$ ). Hence, the biases in the  
560 estimated error and the survey design remain small.

561 Currently, remote sensing technologies (e.g., TLS, Airborne LiDAR, and ground penetrating  
562 radar) are allowing for the characterization of snow cover properties at increasing resolutions in  
563 both space and time. Such improvements can be utilized in the context presented here providing  
564 information about the range of best fitting covariance/correlation models and parameters for  
565 different conditions, supporting the application of methodologies such as the one presented here.  
566 With such improvements, survey designs can be optimized such that estimation errors can be

567 explicitly addressed and accounted for, particularly when extrapolating a limited number of  
568 measurements to estimate the spatial distribution of snow. Such applications will continue to be  
569 relevant despite of the aforementioned improvements, as access to these technologies is limited  
570 by their cost and the expertise that is required for their application.

571

572

573

## **7 Acknowledgements**

574 Data for this article was obtained from NASA's Cold Land Processes experiment (CLPX),

575 available at [http://nsidc.org/data/docs/daac/nsidc0157\\_clpx\\_lidar](http://nsidc.org/data/docs/daac/nsidc0157_clpx_lidar).

576

## Figures

579 Figure 1. (a) Location of the Fraser and Rabbit Ears study areas in the state of Colorado (in  
580 grey). (b) LIDAR Snow depth distributions on April 8, 2003, at the Saint Louis Creek Intensive  
581 Study Area (ISA) and (c) on April 9 at the Rabbit Ears ISA.

582 Figure 2. (a) Sample normalized snow depth profile (mean = 0, standard deviation = 1) in a  
583 forested environment from LIDAR (1-m resolution) at the Fraser – St. Louis Creek (FS)  
584 intensive study area (ISA) of the Cold Land Processes eXperiment (CLPX) (Trujillo et al., 2007;  
585 Cline et al., 2009). The profile is sampled with regular separations (spacing) of 5 m, 10 m, 25 m,  
586 50 m, and 100 m (from top to bottom, respectively). (b) Average values within sampling  
587 intervals (same as in (a)) versus point samples for normalized snow depth profiles in the FS ISA.  
588 The red line is a linear regression fit, with slope  $\beta$  and  $r^2$  as indicated in each plot. (c) Histograms  
589 of the difference between the point and average values for each of the sampling intervals. The  
590 vertical red line marks the mean difference.

591 Figure 3. (a) As Figure 2 but for an open and wind influenced environment at the Rabbit Ears  
592 – Walton Creek (RW) ISA of the CLPX (Trujillo et al., 2007; Cline et al., 2009). (b) Average  
593 values within sampling intervals (same as in (a)) versus point samples for normalized snow depth  
594 profiles in the RW ISA. The red line is a linear regression fit, with slope  $\beta$  and  $r^2$  as indicated in  
595 each plot. (c) Histograms of the difference between the point and average values for each of the  
596 sampling intervals. The vertical red line marks the mean difference.

597 Figure 4. Sub-interval standard deviation (a) and range (b) for varying interval lengths for  
598 profiles of snow depth in a forested environment (FS) and an open and wind-influenced  
599 environment (RW) in the Colorado Rocky Mountains (same regions as those in Figure 2 and  
600 Figure 3). The mean standard deviation and mean range for the study areas are shown by the  
601 solid lines, while the shaded areas cover the quantiles between 25% and 75% of the values for all  
602 the intervals in these areas.

603 Figure 5. Survey designs for the sampling of a snow profile.

604 Figure 6. Comparison of the theoretical and sampled normalized squared error ( $\sigma_z^2/\sigma_p^2$ ) for  
605 the case of a single measurement along a profile section of length  $L$ , as in Figure 5a. The survey  
606 case applied to profiles in FS and RW along the  $x$  and  $y$  directions. Solid lines are the theoretical  
607 error using exponential decay exponents derived from the functions fitted to the sampled  
608 correlation functions of the two surfaces in the  $x$  and  $y$  directions.

609 Figure 7. (a) Theoretical normalized squared error for a single measurement in the middle of a  
610 section of length,  $L$ , and for an exponential correlation function with a decay exponent,  $\nu$ . (b) and  
611 (c) Comparison of the theoretical and sampled normalized squared error for the same survey case  
612 applied to profiles in FS and RW along the  $x$  and  $y$  directions. Dashed lines are the theoretical  
613 error from (7) using exponential decay exponents derived from the functions fitted to the  
614 sampled correlation functions of the two surfaces in the  $x$  and  $y$  directions.

615 Figure 8. (a) and (b) Theoretical normalized squared error for the three-point pattern along a  
616 profile section in Figure 5b, and for profile section lengths ( $L$ ) of 1 (a) and 25 (b). Each of the

617 colored lines corresponds to a specific decay exponent,  $\nu$ , and the black line marks the  
618 theoretical solution for  $a_{optimal}$ . (c) Theoretical normalized error and  $a_{optimal}$  for isolines of profile  
619 section lengths ( $L$ ) and exponential decay exponents ( $\nu$ ) for the three-point pattern along a profile  
620 section of length  $L$  in Figure 5b.

621 Figure 9. Theoretical and sampled normalized squared error ( $\sigma_z^2/\sigma_p^2$ ) for the three-point  
622 pattern along a profile section in Figure 5b, and for profile section lengths ( $L$ ) between 10 m and  
623 80 m in FS and RW. The solid lines are the theoretical error from (8) using exponential decay  
624 exponents derived from the functions fitted to the sampled correlation functions of the two  
625 surfaces in the  $x$  and  $y$  directions, while the dots correspond to the sampled error for profiles in  
626 FS (a-d) and RW (e-h).

627 Figure 10. Theoretical normalized squared error ( $\sigma_z^2/\sigma_p^2$ ) for the  $N$ -point pattern along a  
628 profile section in Figure 5c, and for profile section lengths ( $L$ ) between 10 and 80 obtained from  
629 (10).

630 Figure 11. Theoretical and sampled normalized squared error ( $\sigma_z^2/\sigma_p^2$ ) for the  $N$ -point pattern  
631 along a profile section in Figure 5c, and for profile section lengths ( $L$ ) between 10 m and 80 m in  
632 FS and RW. The solid point markers are the theoretical error from (10) using exponential decay  
633 exponents derived from the functions fitted to the sampled correlograms of the two surfaces in  
634 the  $x$  and  $y$  directions, while the circle markers with the dotted lines correspond to the sampled  
635 error for profiles in FS (a-d) and RW (e-h).

636 Figure 12. Sample survey designs with (a) a 5-point pattern centered in the area, and (b) a  
637 regularly spaced pattern. For the 5-point pattern,  $a$  can vary between 0 and  $L/2$ , while for the  $N \times$   
638  $N$  points pattern, the separation between the measurements is determined by the number of  
639 points.

640 Figure 13. (a) Theoretical normalized squared error ( $\sigma_z^2/\sigma_p^2$ ) for the two-dimensional case  
641 with a single measurement in the middle of a square area with side dimension  $L$ . (b) Theoretical  
642 and sampled normalized squared error for the same two-dimensional survey applied to the snow  
643 depth field in FS. The dashed line is the theoretical error derived for an exponential decay  
644 exponent of 0.17 derived from the sampled correlation function of snow depth in FS, while the  
645 solid line is the sampled normalized squared error for the snow cover in FS.

646 Figure 14. Theoretical normalized squared error ( $\sigma_z^2/\sigma_p^2$ ) as a function of the distance  $a$  from  
647 the center of the area for square areas of side dimensions ( $L$ ) between 10 and 80. Each curve  
648 corresponds to an exponential decay ( $\nu$ ) between 0.1 and 5.

649 Figure 15. Theoretical and sampled normalized squared error ( $\sigma_z^2/\sigma_p^2$ ) for the 5-point pattern  
650 in Figure 12a over square areas of side dimensions ( $L$ ) between 10.7 m and 79.1 m. The  
651 separation distance ( $a$ ) is varied from the center outwards. The solid line is the theoretical error  
652 derived for an exponential decay exponent of 0.17 derived from the sampled correlation function  
653 of snow depth in FS, while the solid red point markers are the sampled normalized squared error  
654 for the snow cover in FS.

655 Figure 16. Theoretical normalized squared error ( $\sigma_z^2/\sigma_p^2$ ) for the  $N$  by  $N$  point pattern in  
656 Figure 12b, and for areas of side dimension ( $L$ ) between 10 and 80. The exponential exponent is  
657 varied between 0.1 and 5.

658 Figure 17. Theoretical and sampled normalized squared error ( $\sigma_z^2/\sigma_p^2$ ) for the  $N$  by  $N$  point  
659 pattern in Figure 12b, and over square areas of side dimensions ( $L$ ) between 10.7 m and 79.1 m.  
660 The solid black point markers are the theoretical error for an exponential decay exponent of 0.17  
661 derived from the sampled correlogram of snow depth in FS. The dotted red lines with circle  
662 markers are the sampled normalized squared error for the snow cover in FS.

663

664



- 666 Blöschl, G.: Scaling issues in snow hydrology, *Hydrol. Processes*, 13(14-15), 2149-2175, 1999.
- 667 Chang, A. T. C., Kelly, R. E. J., Josberger, E. G., Armstrong, R. L., Foster, J. L., and Mognard,  
668 N. M.: Analysis of ground-measured and passive-microwave-derived snow depth variations in  
669 midwinter across the northern Great Plains, *J. Hydrometeor.*, 6(1), 20-33, doi: 10.1175/Jhm-  
670 405.1, 2005.
- 671 Cline, D., Yueh, S., Chapman, B., Stankov, B., Gasiewski, A., Masters, D., Elder, K., Kelly, R.,  
672 Painter, T. H., Miller, S., Katzberg, S., and Mahrt, L.: NASA Cold Land Processes Experiment  
673 (CLPX 2002/03): Airborne Remote Sensing, *J. Hydrometeor.*, 10(1), 338-346, 2009.
- 674 Cressie, N.: *Statistics for spatial data*, 900 pp., John Wiley & Sons, Inc., USA, 1993.
- 675 Deems, J. S., Fassnacht, S. R., and Elder, K. J.: Interannual Consistency in Fractal Snow Depth  
676 Patterns at Two Colorado Mountain Sites, *J. Hydrometeor.*, 9(5), 977-988, doi:  
677 10.1175/2008jhm901.1, 2008.
- 678 Grünewald, T., and Lehning, M.: Are flat-field snow depth measurements representative? A  
679 comparison of selected index sites with areal snow depth measurements at the small catchment  
680 scale, *Hydrol. Processes*, doi: 10.1002/hyp.10295, 2014.
- 681 Helfrich, K., Schöber, J., Schneider, K., Sailer, R., and Kuhn, M.: Interannual persistence of the  
682 seasonal snow cover in a glacierized catchment, *J. Glaciol.*, 60(223), 889-904, doi:  
683 10.3189/2014JG13J197, 2014.
- 684 Journel, A. G., and Huijbregts, C. J.: *Mining Geostatistics*, Academic Press, London, 1978.
- 685 Kronholm, K., and Birkeland, K. W.: Reliability of sampling designs for spatial snow surveys,  
686 *Comput. Geosci.*, 33(9), 1097-1110, 2007.
- 687 Lopez-Moreno, J. I., Fassnacht, S. R., Begueria, S., and Latron, J. B. P.: Variability of snow  
688 depth at the plot scale: implications for mean depth estimation and sampling strategies,  
689 *Cryosphere*, 5(3), 617-629, 2011.
- 690 Matheron, G.: Application des méthodes statistiques à l'estimation des gisements, *Annales de*  
691 *Mines, Dec*, 50-75, 1955.
- 692 Matheron, G.: Random functions, and their applications in geology, in *Geostatistics - A*  
693 *colloquium*, edited by D. Merriam, pp. 79-87, Plenum Press, New York, 1970.
- 694 Melvold, K., and Skaugen, T.: Multiscale spatial variability of lidar-derived and modeled snow  
695 depth on Hardangervidda, Norway, *Ann. Glaciol.*, 54(62), 273-281, 2013.
- 696 Meromy, L., Molotch, N. P., Link, T. E., Fassnacht, S. R., and Rice, R.: Subgrid variability of  
697 snow water equivalent at operational snow stations in the western USA, *Hydrol. Processes*,  
698 27(17), 2383-2400, doi: 10.1002/Hyp.9355, 2013.
- 699 Mott, R., Schirmer, M., and Lehning, M.: Scaling properties of wind and snow depth distribution  
700 in an Alpine catchment, *Journal of Geophysical Research: Atmospheres*, 116(D6), D06106, doi:  
701 10.1029/2010jd014886, 2011.

702 Rice, R., and Bales, R. C.: Embedded-sensor network design for snow cover measurements  
703 around snow pillow and snow course sites in the Sierra Nevada of California, *Water Resour.*  
704 *Res.*, *46*, W03537, doi: 10.1029/2008wr007318, 2010.

705 Rodríguez-Iturbe, I., and Mejía, J. M.: Design of Rainfall Networks in Time and Space, *Water*  
706 *Resour. Res.*, *10*(4), 713-728, 1974.

707 Schirmer, M., Wirz, V., Clifton, A., and Lehning, M.: Persistence in intra-annual snow depth  
708 distribution: 1. Measurements and topographic control, *Water Resour. Res.*, *47*(9), W09516, doi:  
709 10.1029/2010wr009426, 2011.

710 Shea, C., and Jamieson, B.: Star: an efficient snow point-sampling method, *Ann. Glaciol.*,  
711 *51*(54), 64-72, 2010.

712 Skøien, J. O., and Blöschl, G.: Sampling scale effects in random fields and implications for  
713 environmental monitoring, *Environ. Monit. Assess.*, *114*(1-3), 521-552, doi: Doi  
714 10.1007/S10661-006-4939-Z, 2006.

715 Sturm, M., and Wagner, A. M.: Using repeated patterns in snow distribution modeling: An  
716 Arctic example, *Water Resour. Res.*, *46*, 2010.

717 Trujillo, E., Ramirez, J. A., and Elder, K. J.: Topographic, meteorologic, and canopy controls on  
718 the scaling characteristics of the spatial distribution of snow depth fields, *Water Resour. Res.*, *43*,  
719 W07409, doi: 10.1029/2006WR005317, 2007.

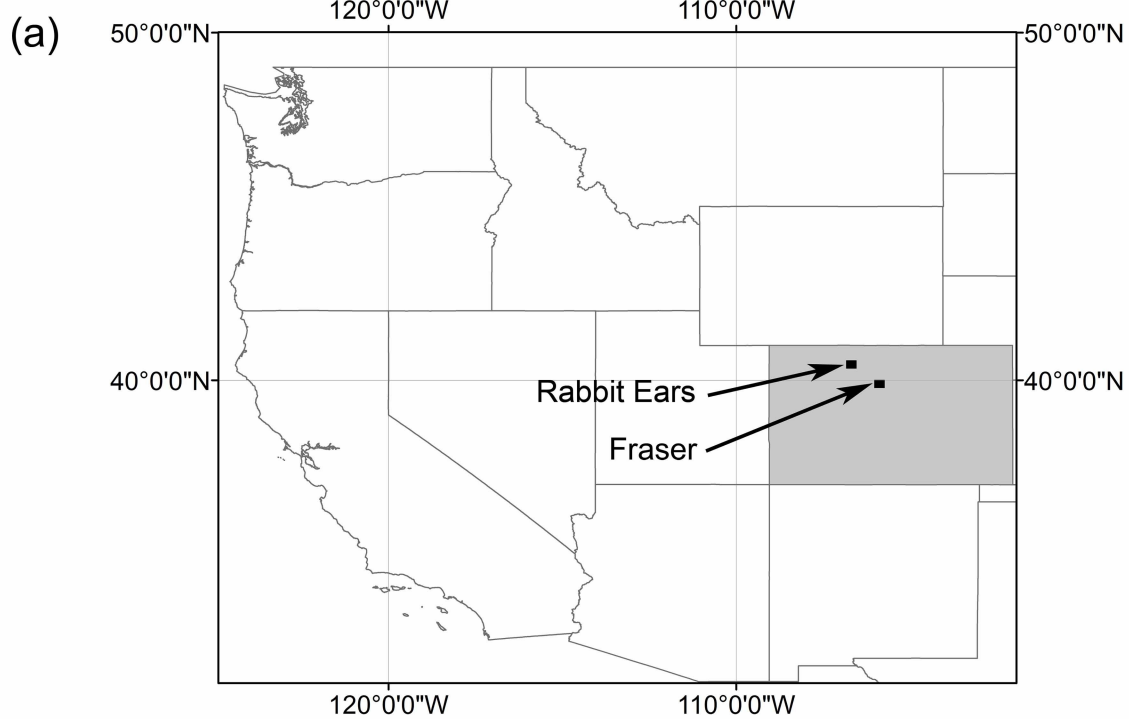
720 Trujillo, E., Ramírez, J. A., and Elder, K. J.: Scaling properties and spatial organization of snow  
721 depth fields in sub-alpine forest and alpine tundra, *Hydrol. Processes*, *23*, 1575–1590, doi:  
722 10.1002/hyp.7270, 2009.

723 Watson, F. G. R., Anderson, T. N., Newman, W. B., Alexander, S. E., and Garrott, R. A.:  
724 Optimal sampling schemes for estimating mean snow water equivalents in stratified  
725 heterogeneous landscapes, *J. Hydrol.*, *328*(3-4), 432-452, doi: 10.1016/J.Jhydrol.2005.12.032,  
726 2006.

727 Yang, D. Q., and Woo, M. K.: Representativeness of local snow data for large scale hydrologic  
728 investigations, *Hydrol. Processes*, *13*(12-13), 1977-1988, doi: 10.1002/(Sici)1099-  
729 1085(199909)13:12/13<1977::Aid-Hyp894>3.0.Co;2-B, 1999.

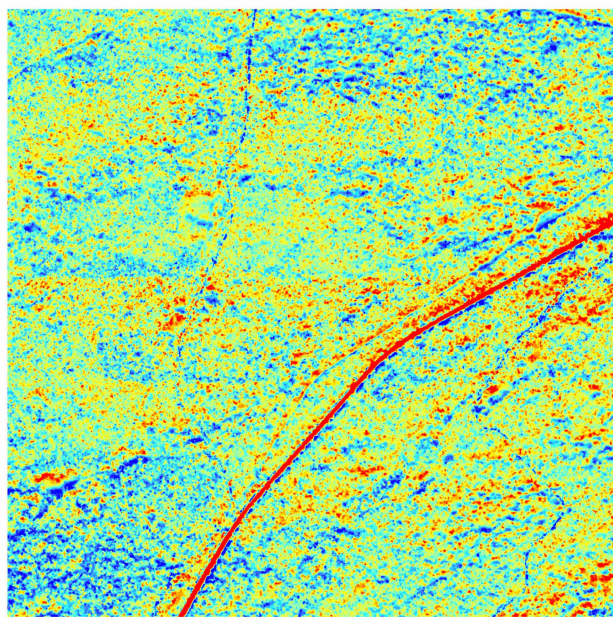
730

731

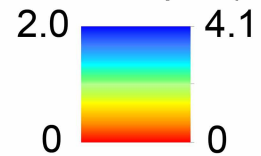


(b) Fraser - St. Louis Creek

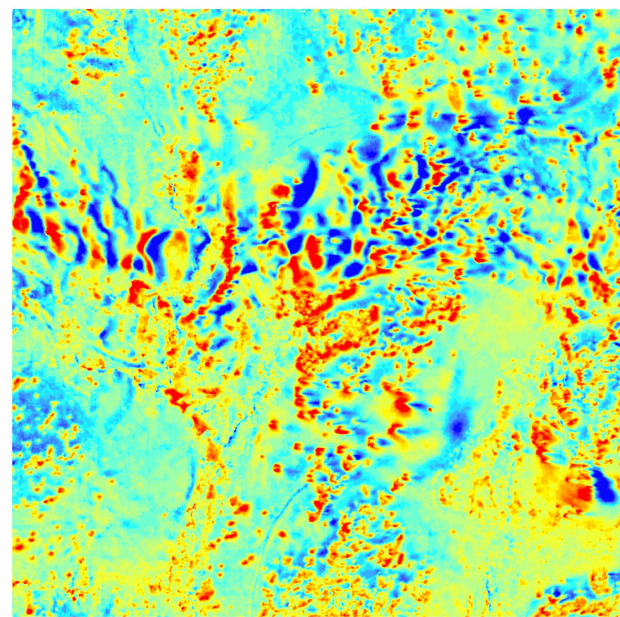
0 125 250 500 Meters

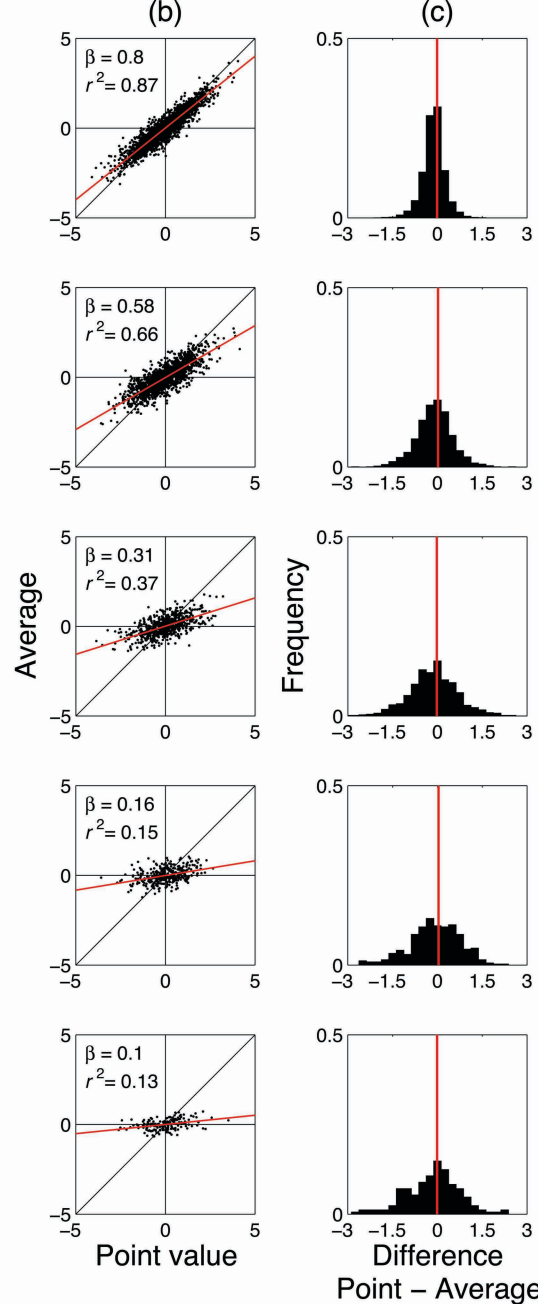
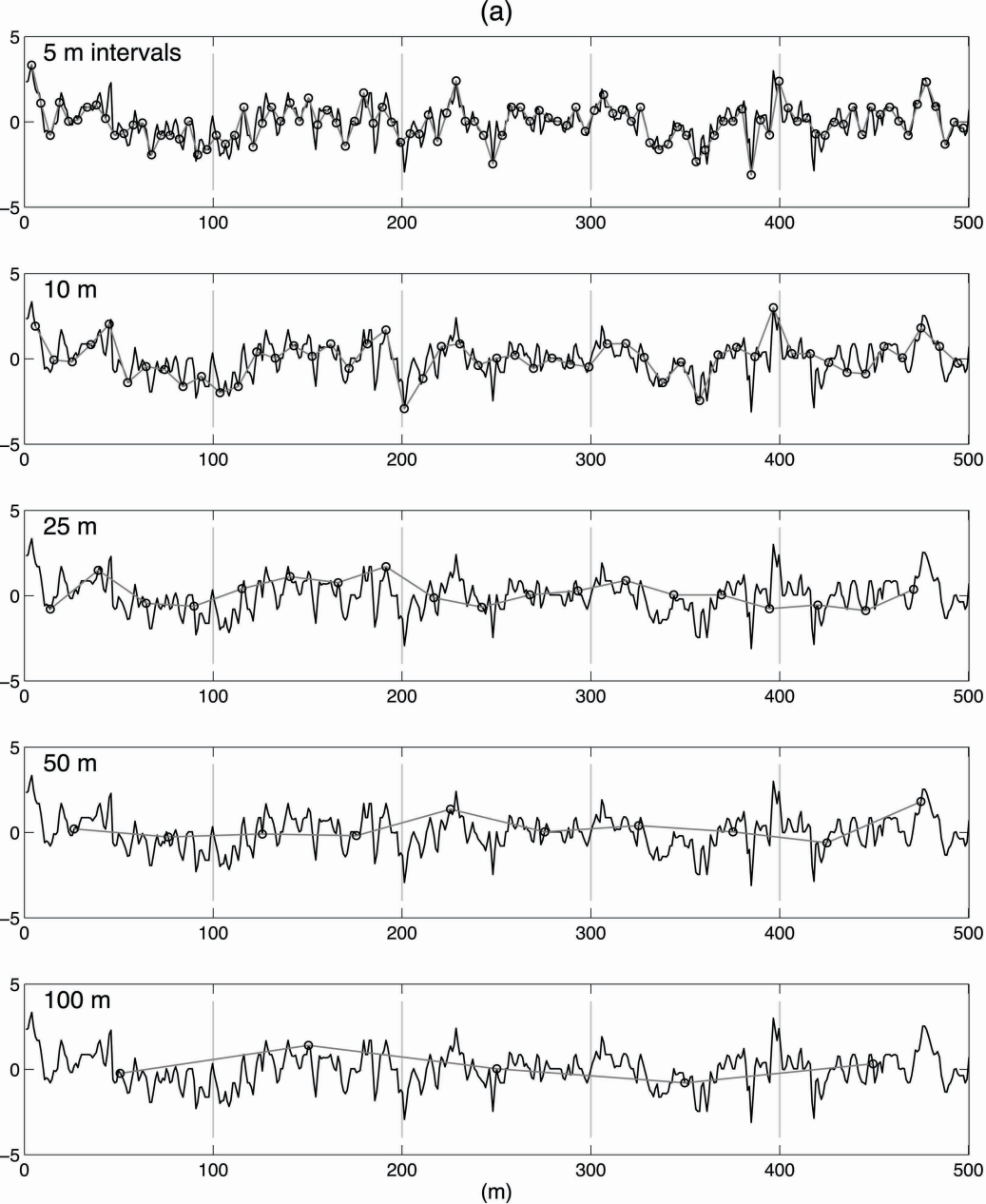


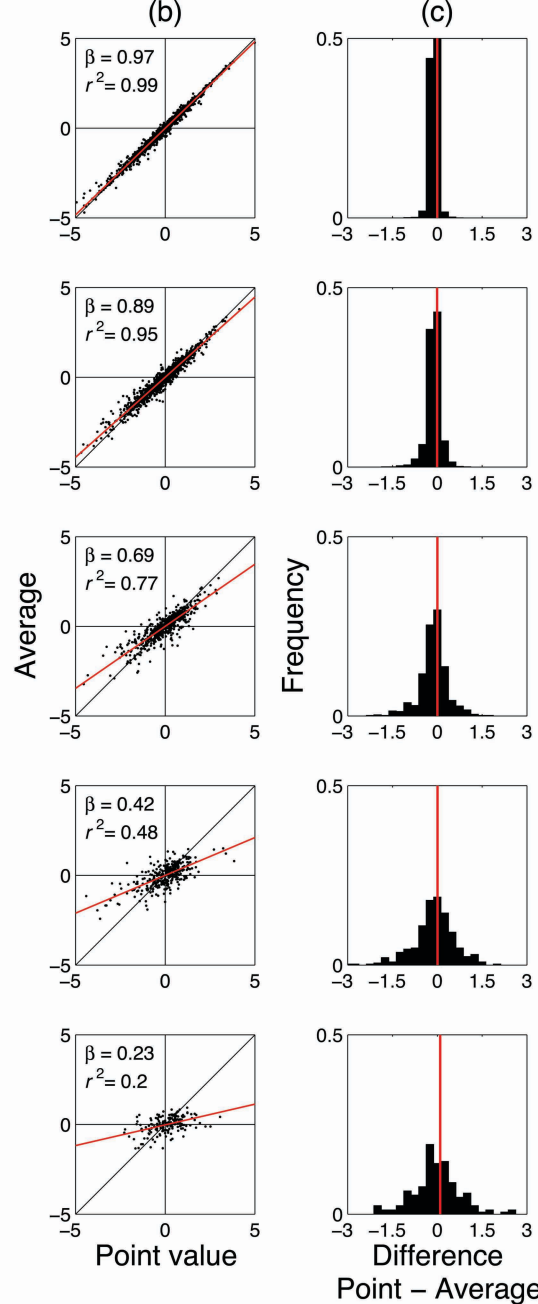
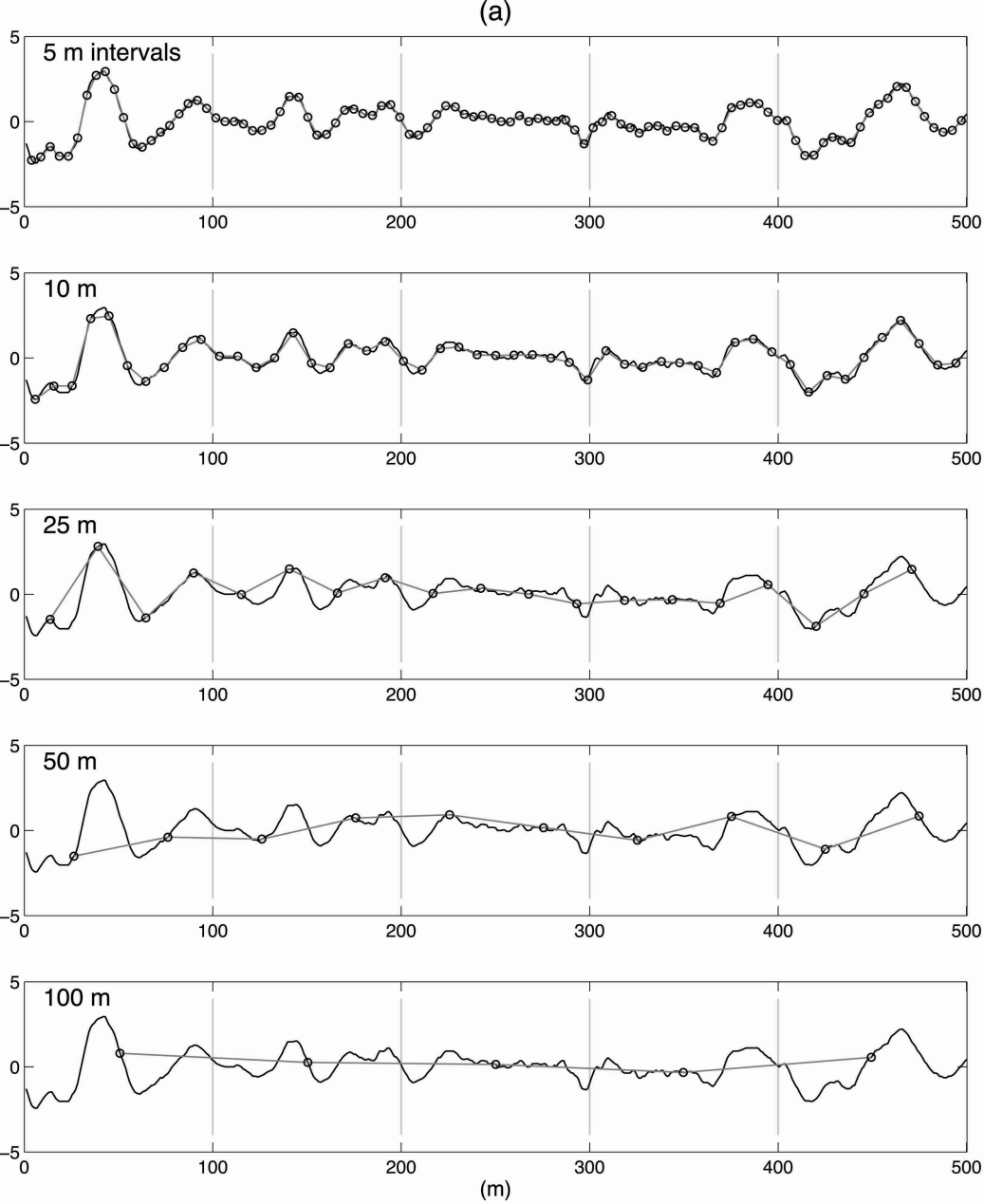
Snow depth (m)



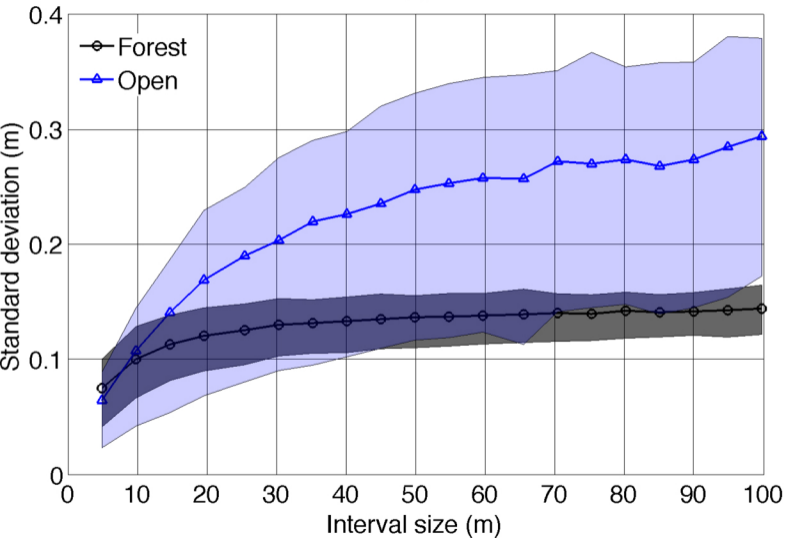
(c) Rabbit Ears - Walton Creek



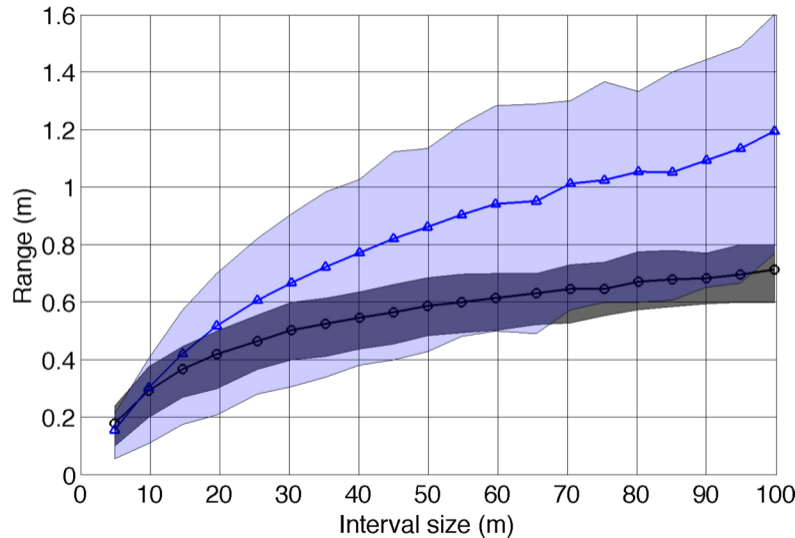




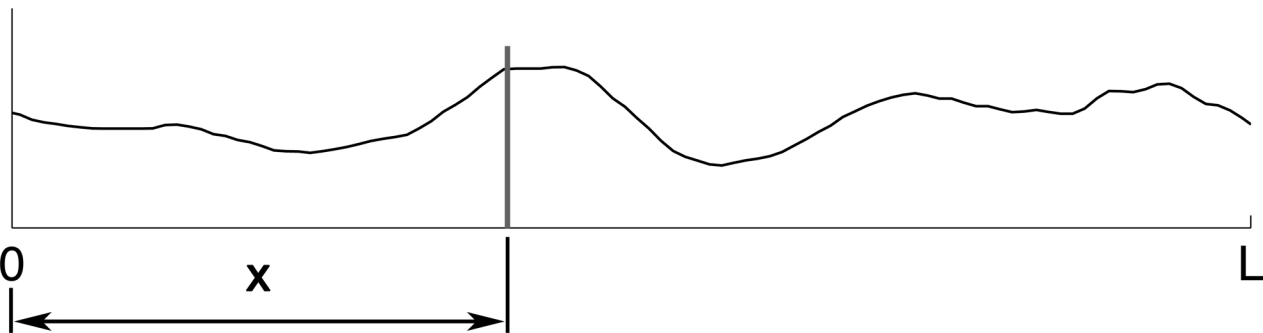
(a)



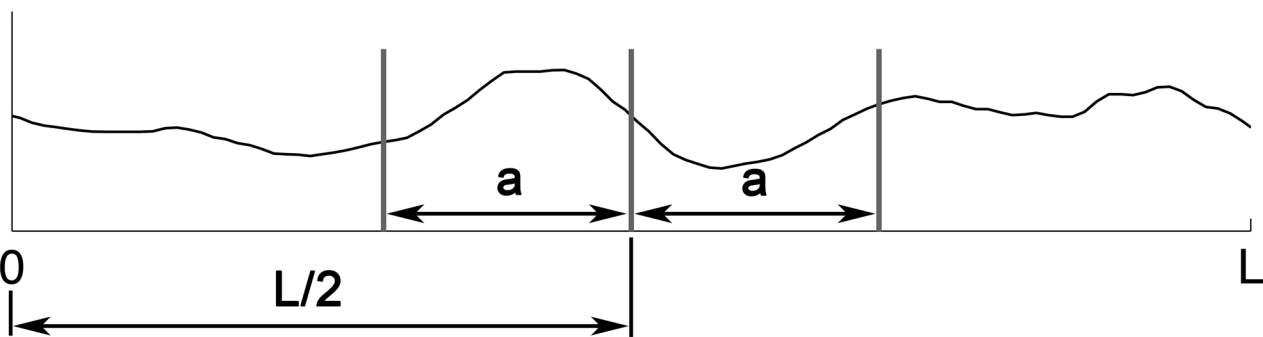
(b)



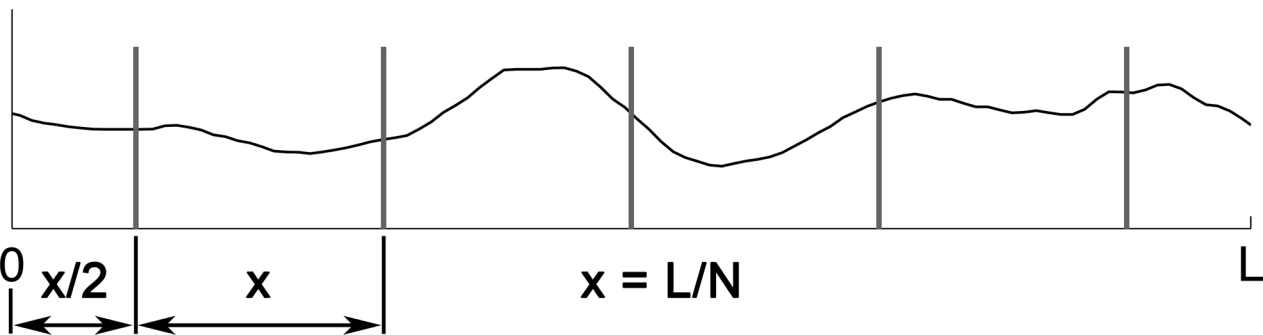
(a) One measurement

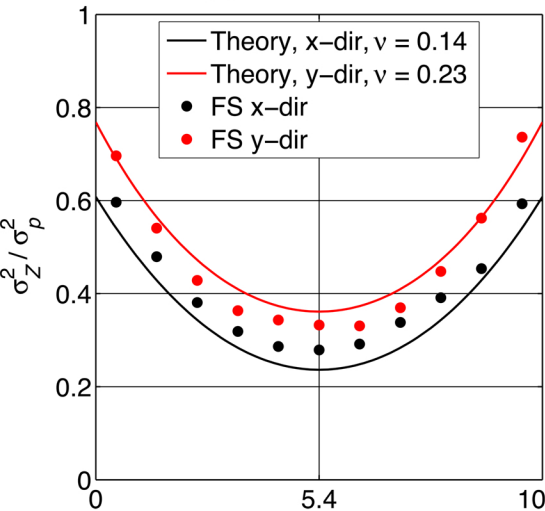
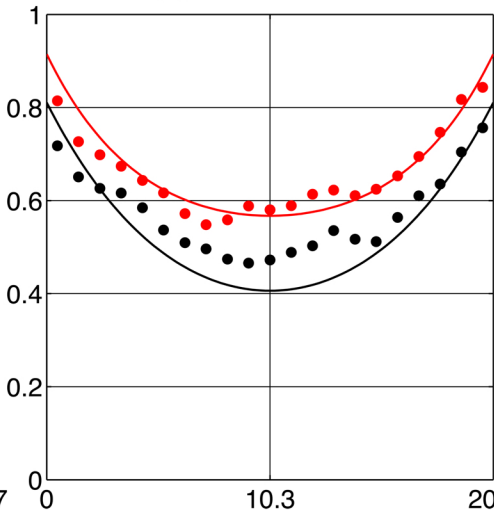
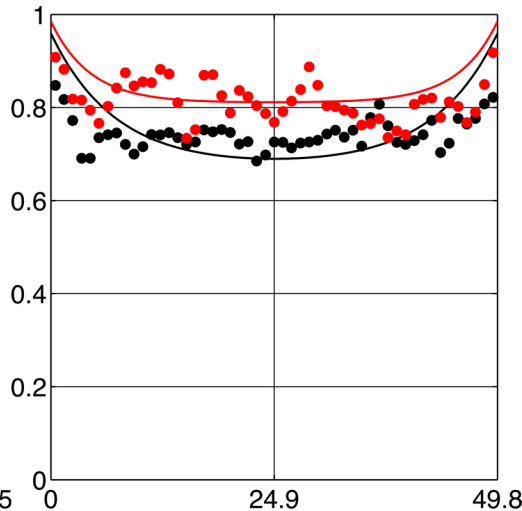
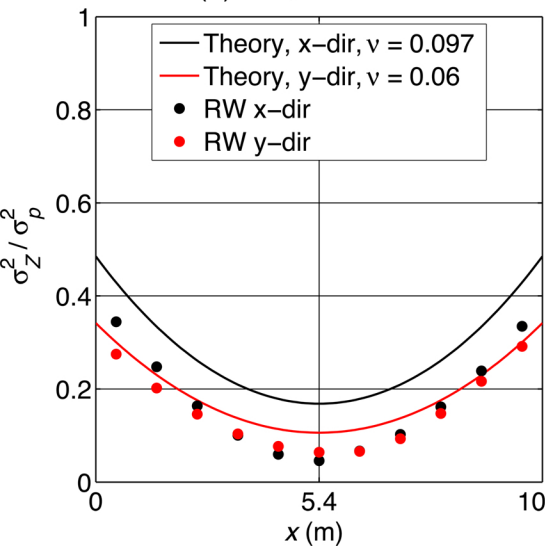
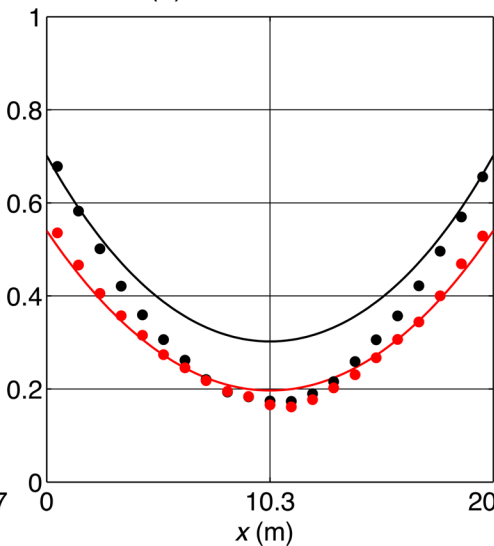
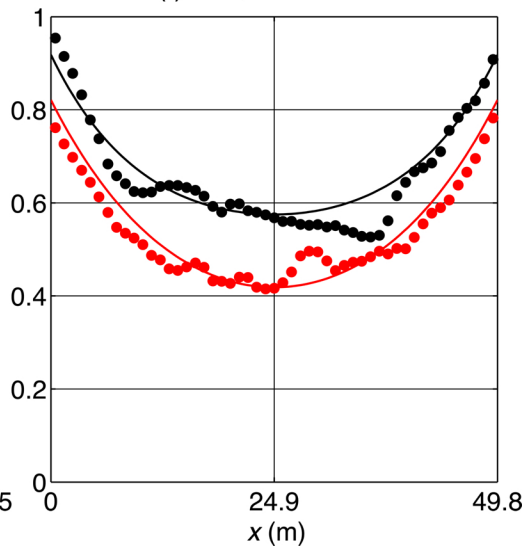


(b) Three measurements



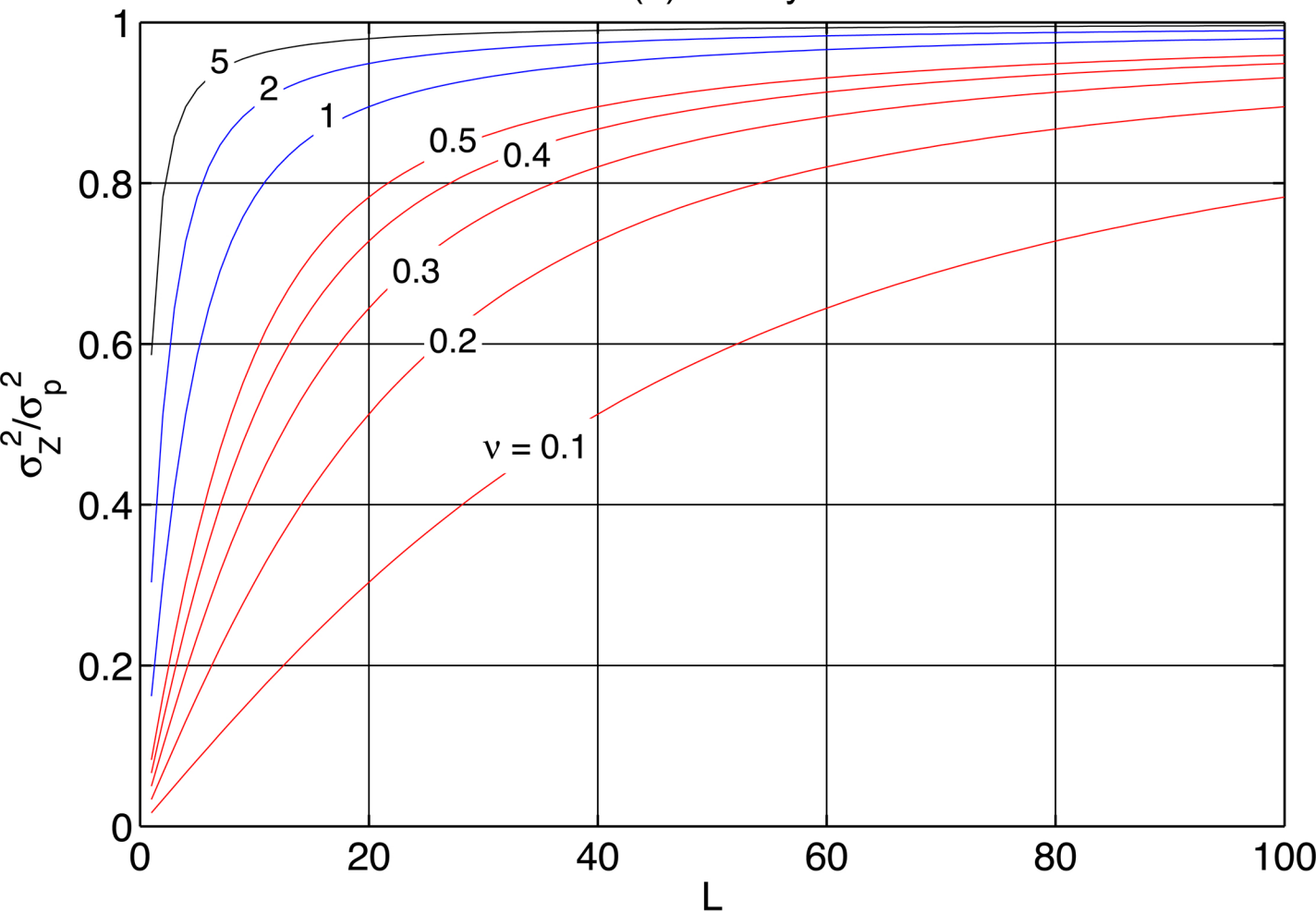
(c)  $N$  measurements



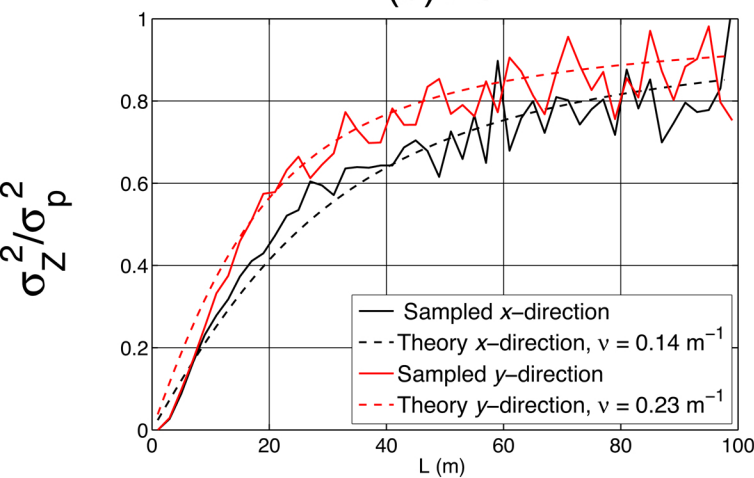
(a) FS,  $L = 10.7$  m(b) FS,  $L = 20.5$  m(c) FS,  $L = 49.8$  m(d) RW,  $L = 10.7$  m(e) RW,  $L = 20.5$  m(f) RW,  $L = 49.8$  m



(a) Theory

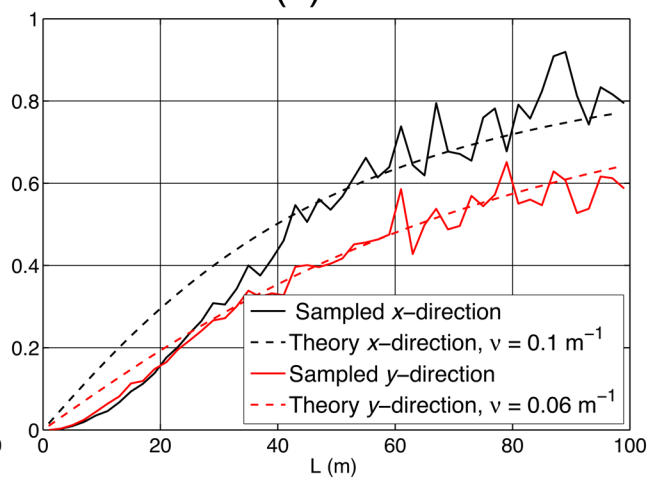


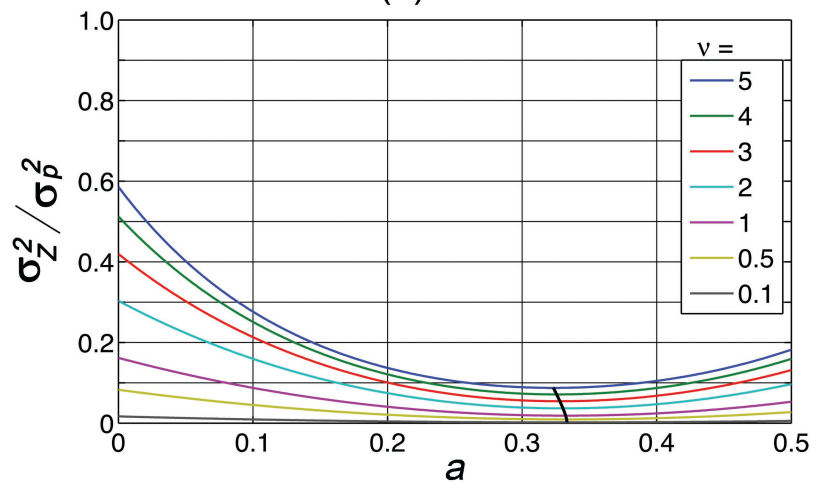
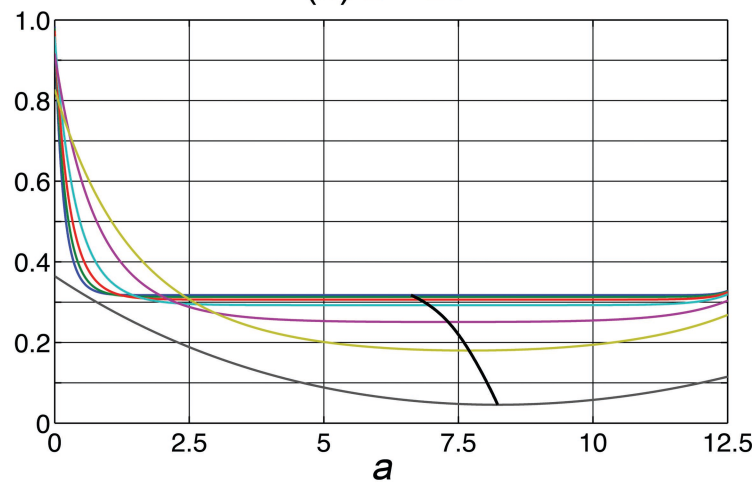
(b) FS



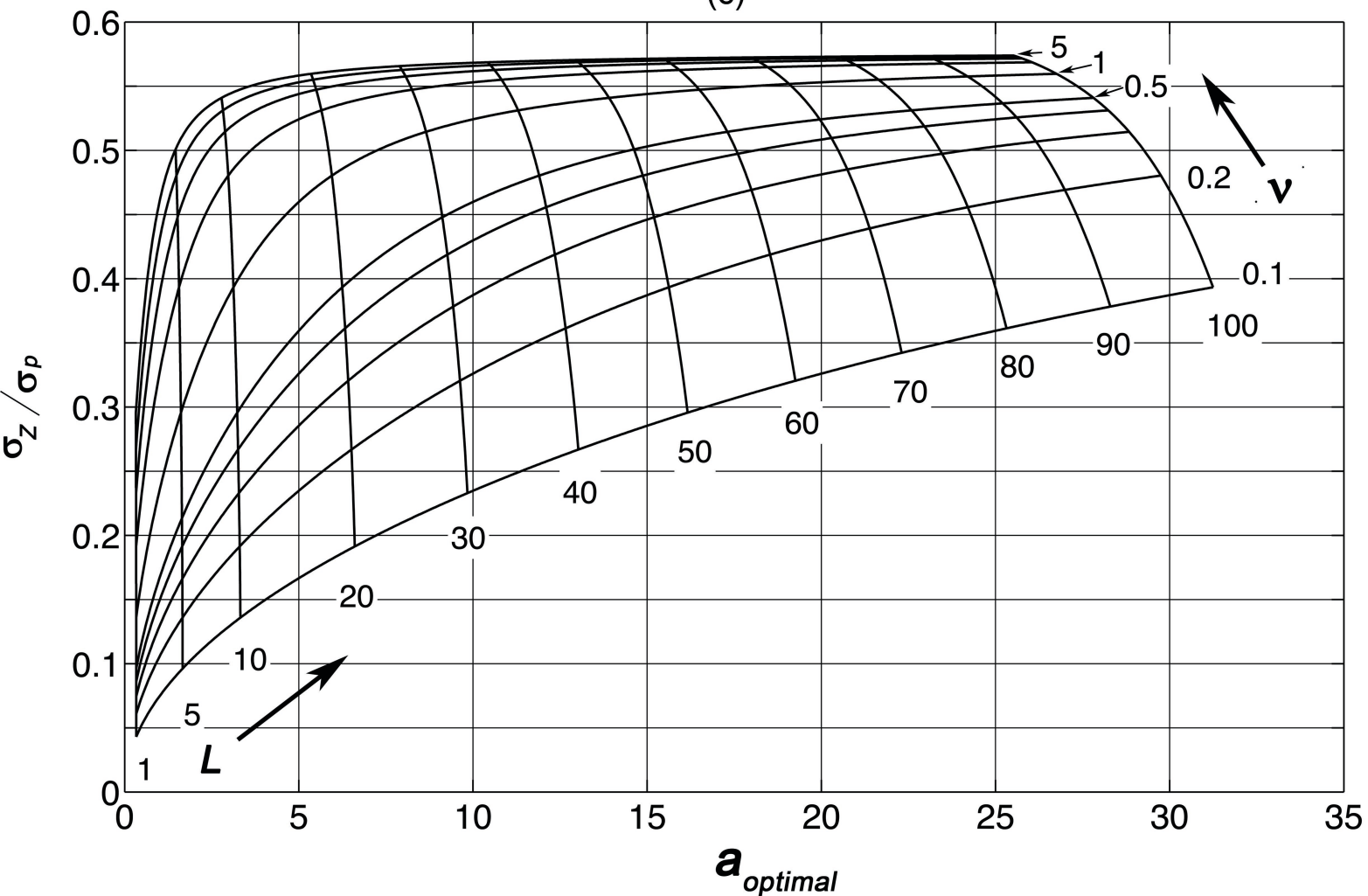
L

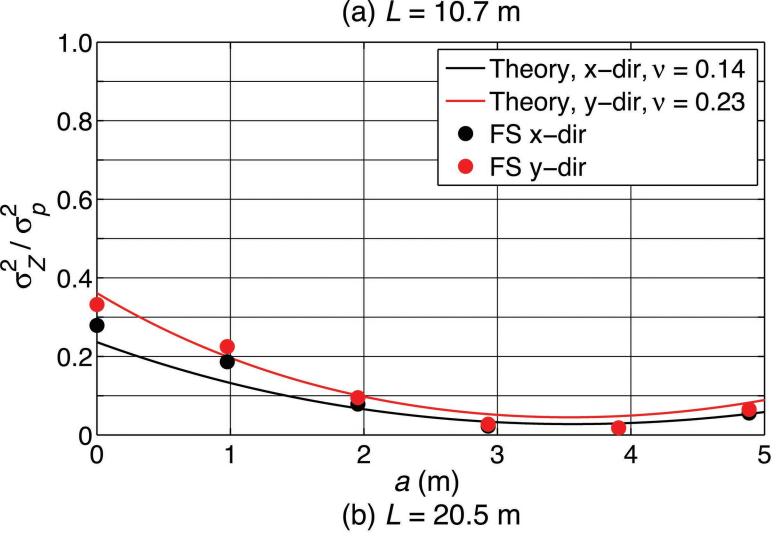
(c) RW



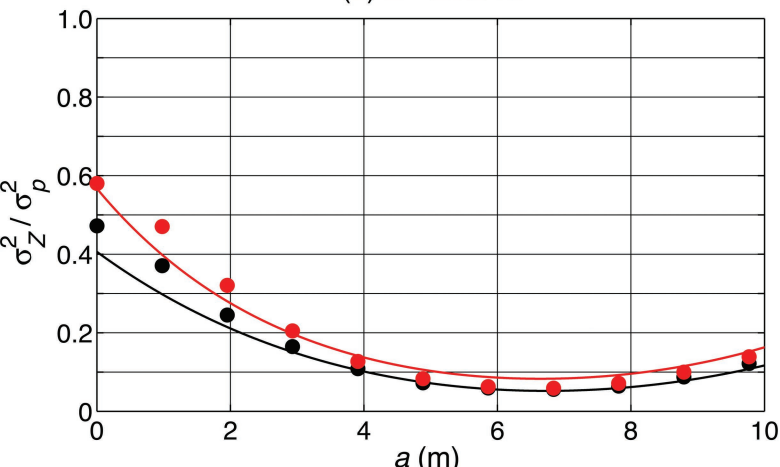
(a)  $L = 1$ (b)  $L = 25$ 

(c)

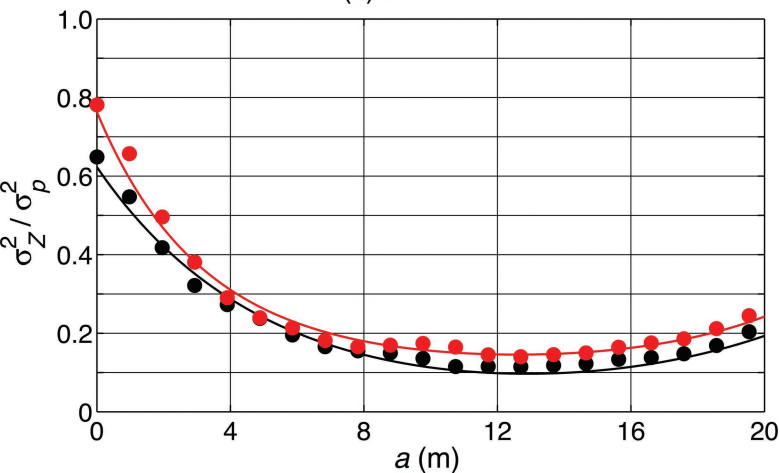




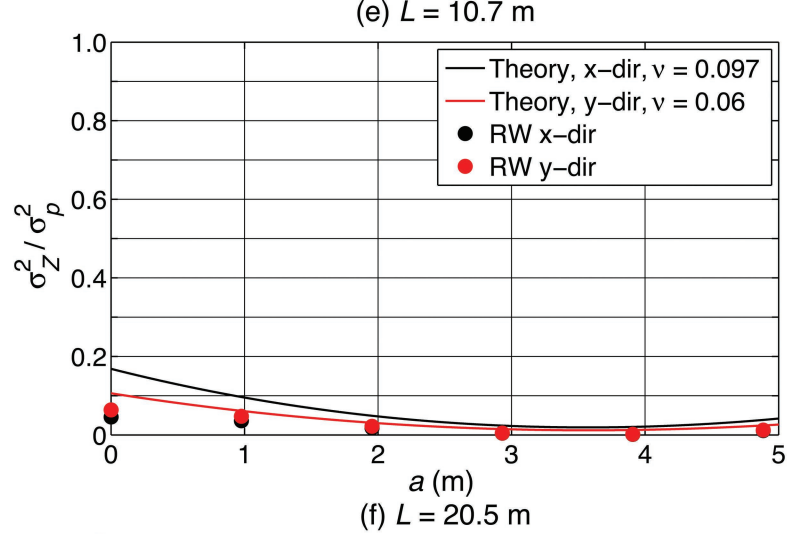
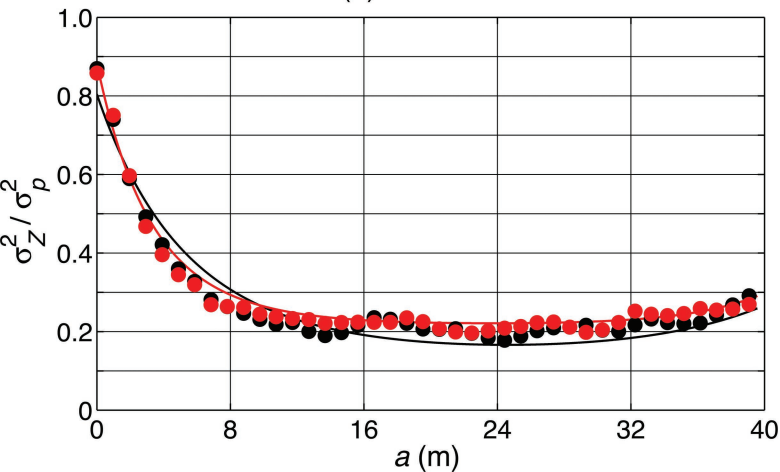
(b)  $L = 20.5$  m



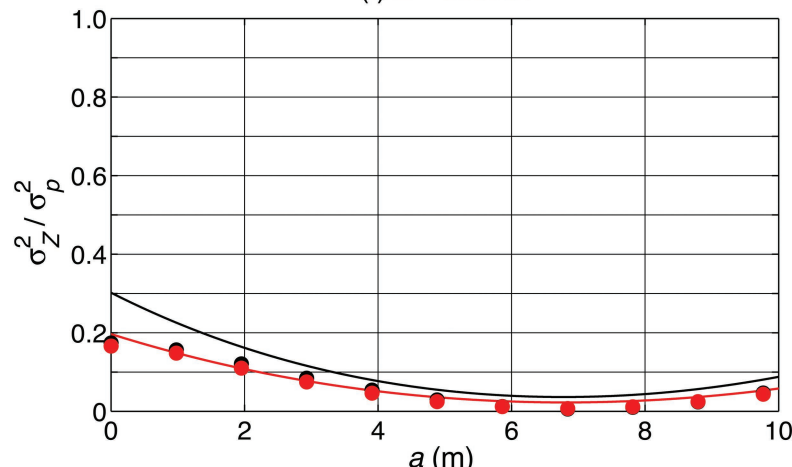
(c)  $L = 40.1$  m



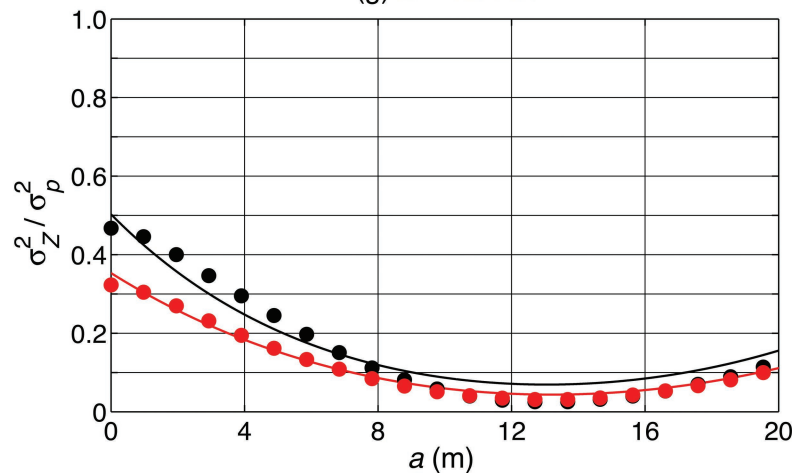
(d)  $L = 79.1$  m



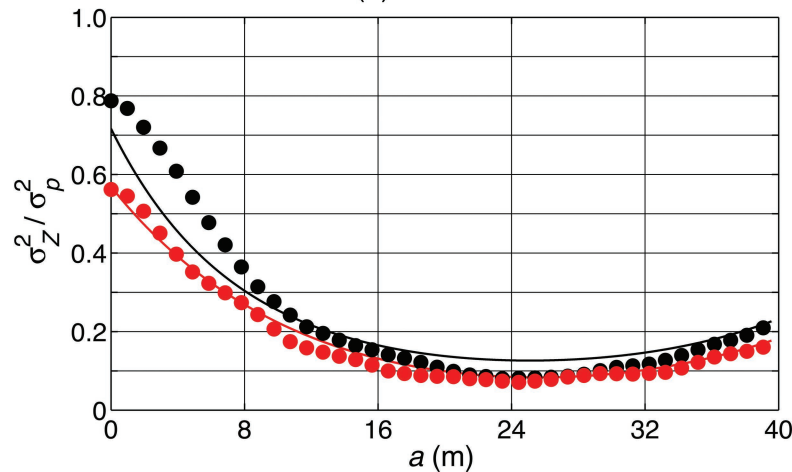
(f)  $L = 20.5$  m

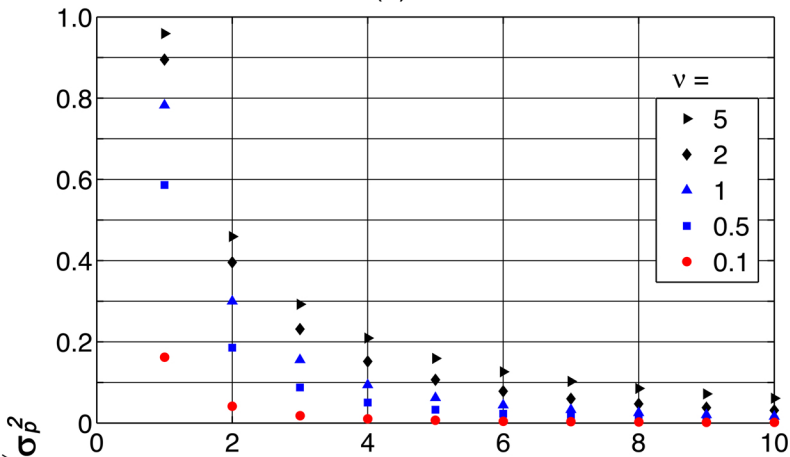
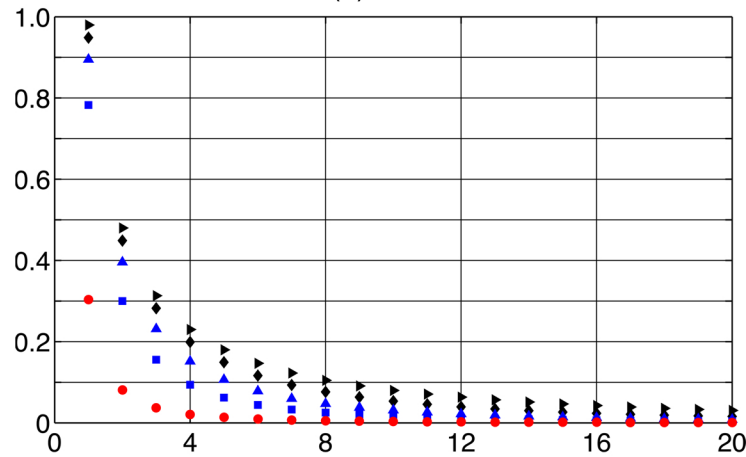
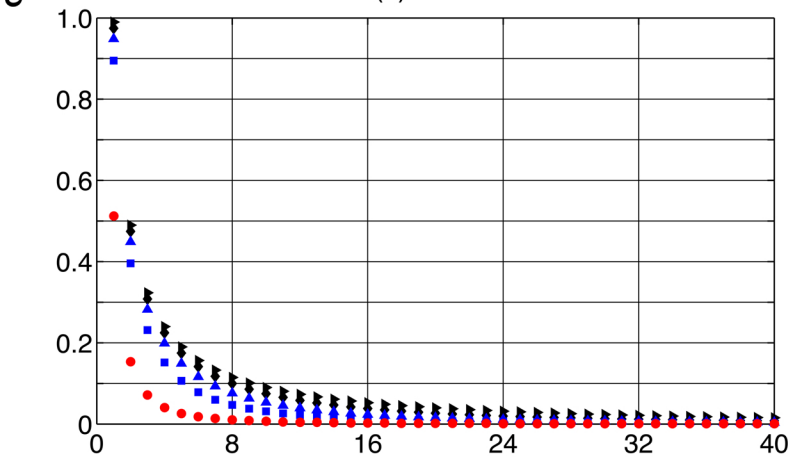
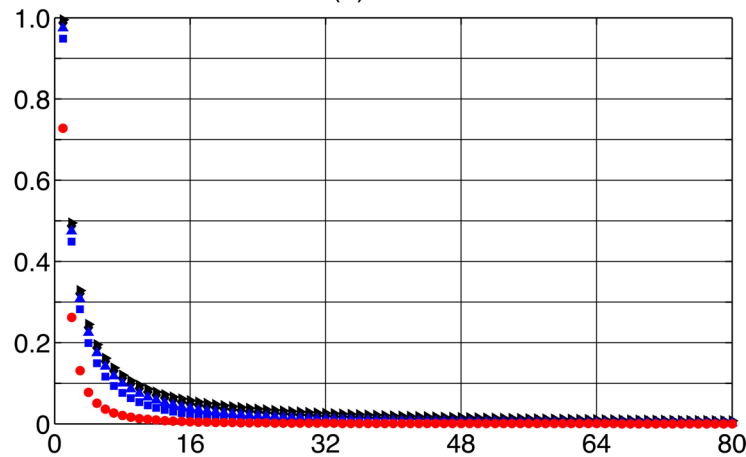


(g)  $L = 40.1$  m

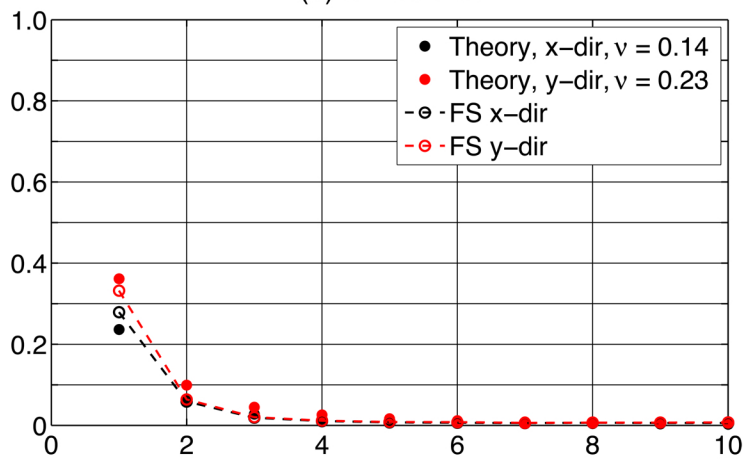
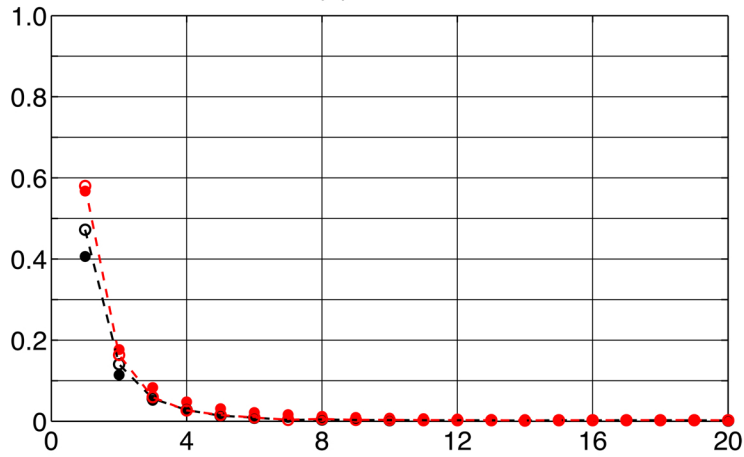
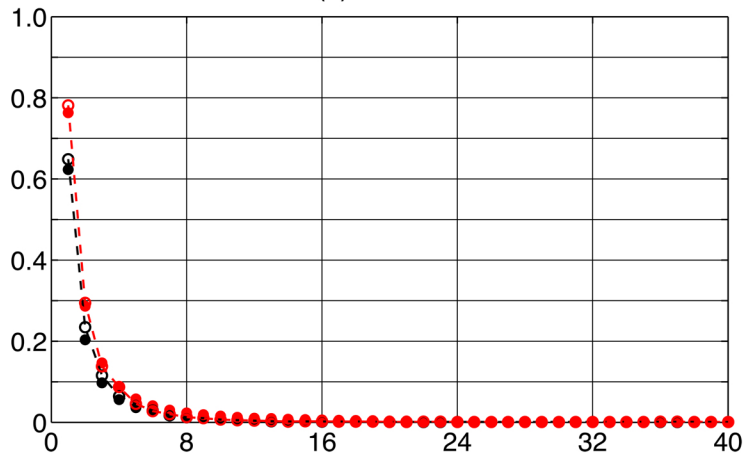
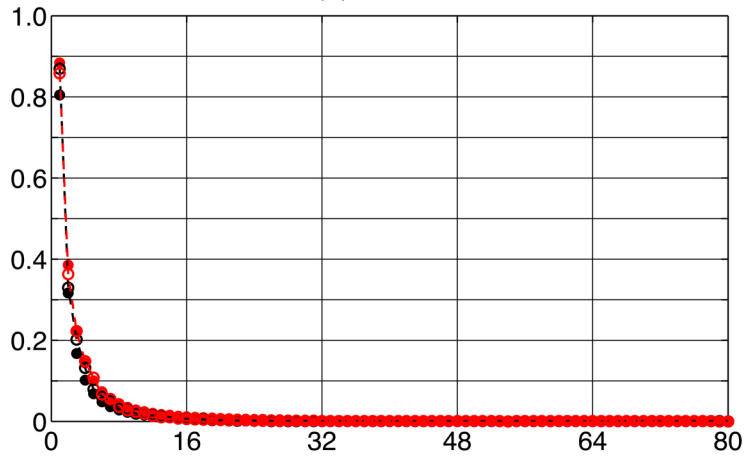
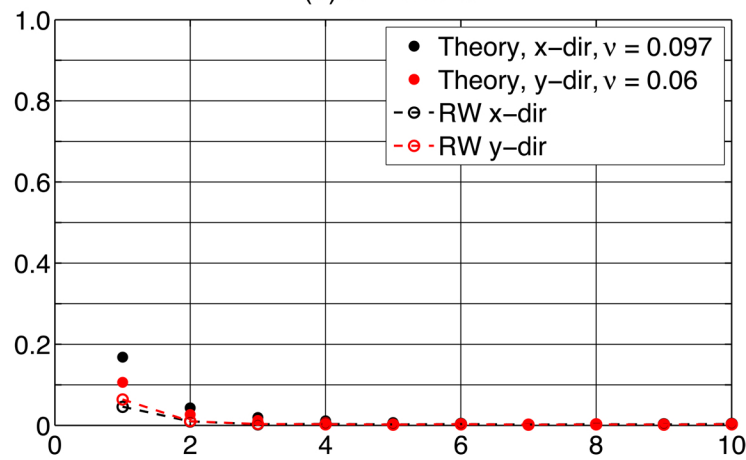
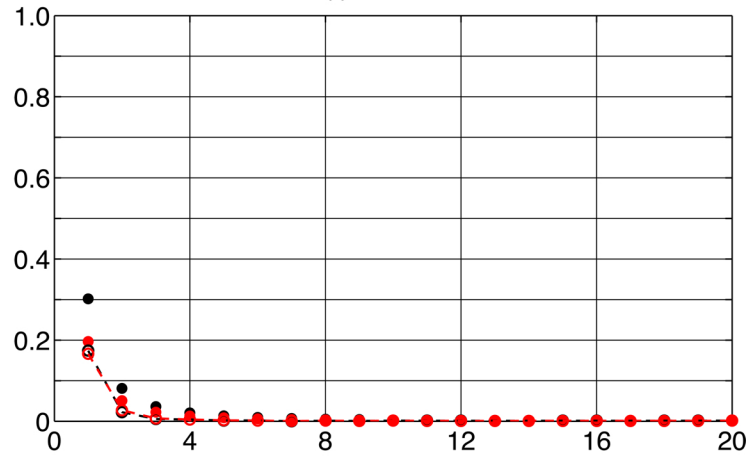
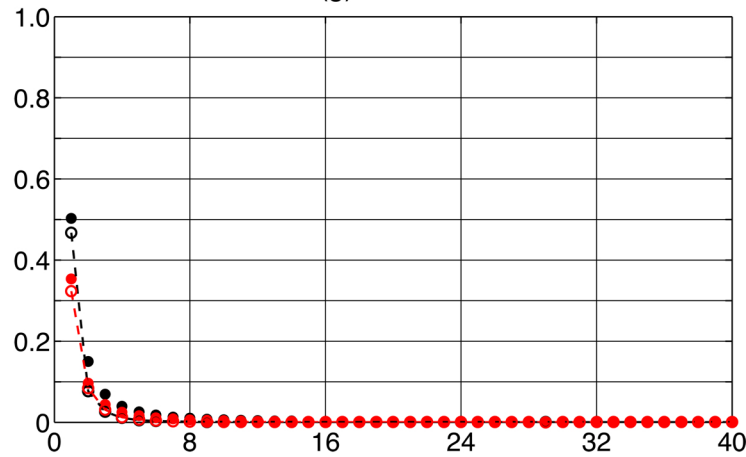
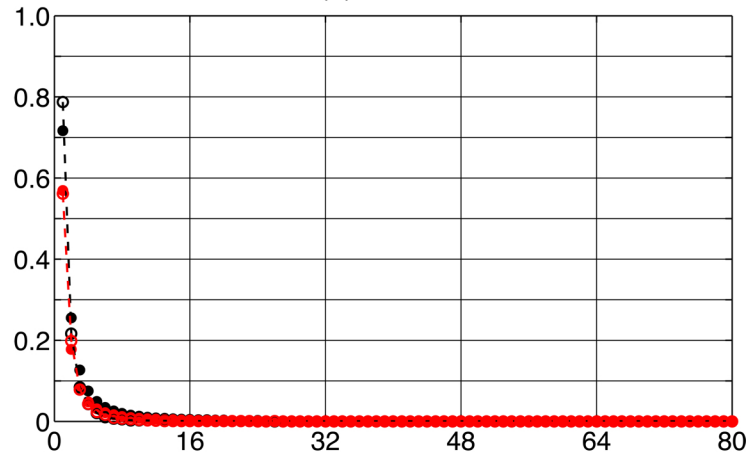


(h)  $L = 79.1$  m



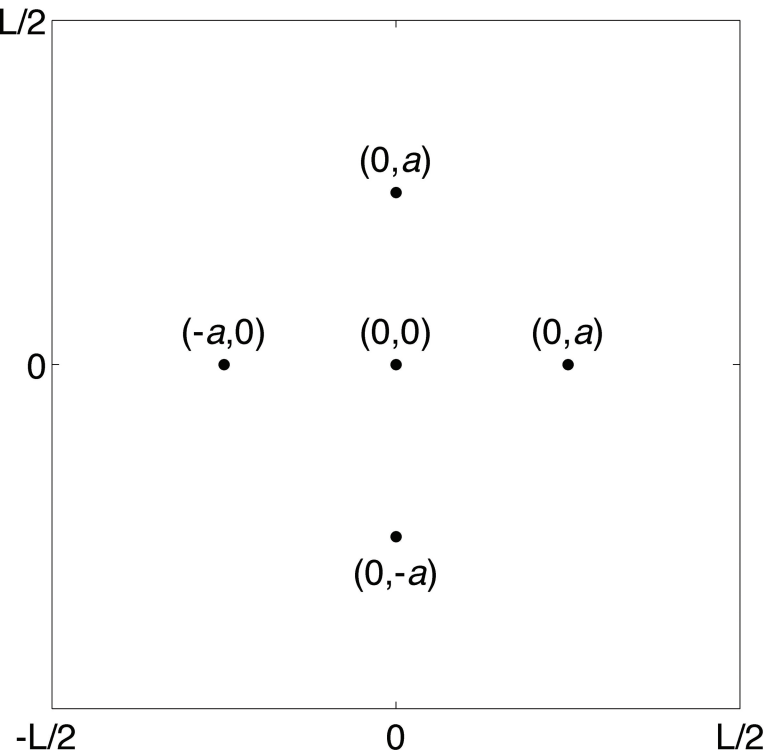
(a)  $L = 10$ (b)  $L = 20$ (c)  $L = 40$ (d)  $L = 80$ 

Number of Point Measurements

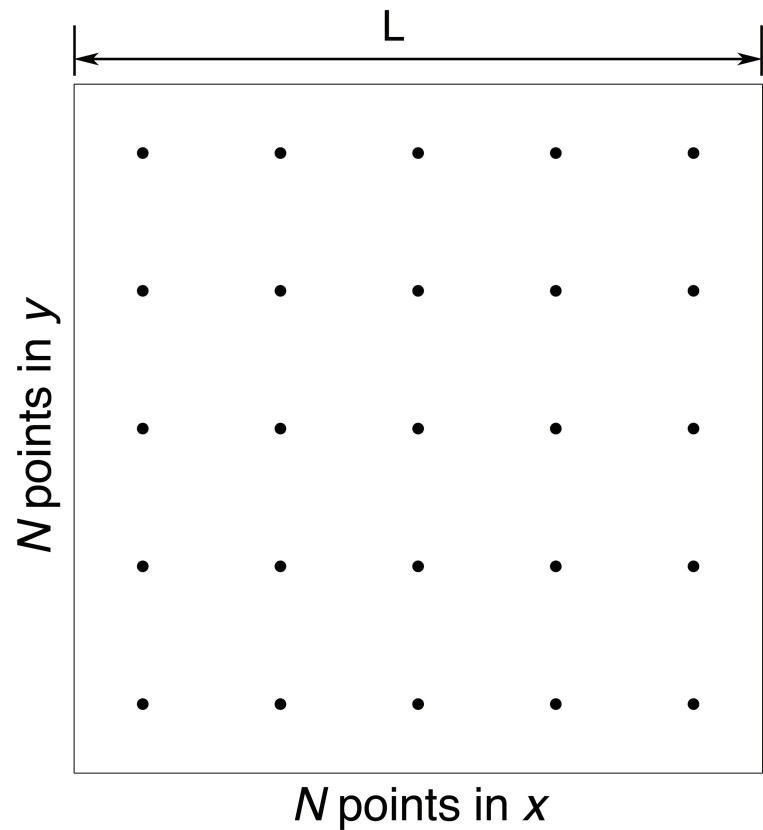
(a)  $L = 10.7$  m(b)  $L = 20.5$ (c)  $L = 40.1$ (d)  $L = 79.1$ (e)  $L = 10.7$  m(f)  $L = 20.5$ (g)  $L = 40.1$ (h)  $L = 79.1$ 

Number of Point Measurements

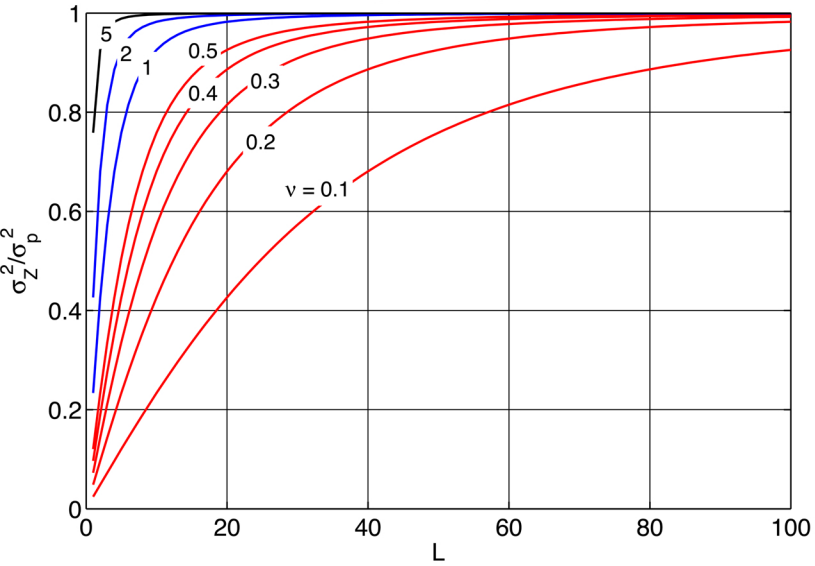
(a) 5 Points



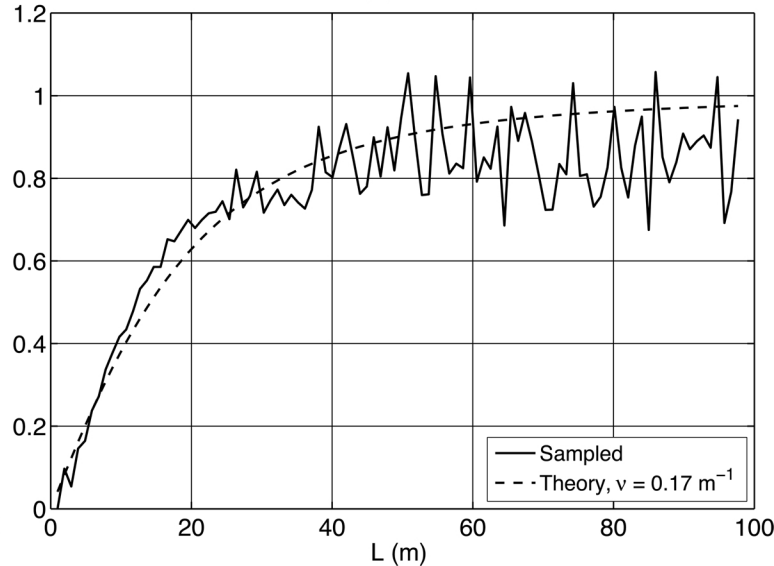
(b)  $N \times N$  points



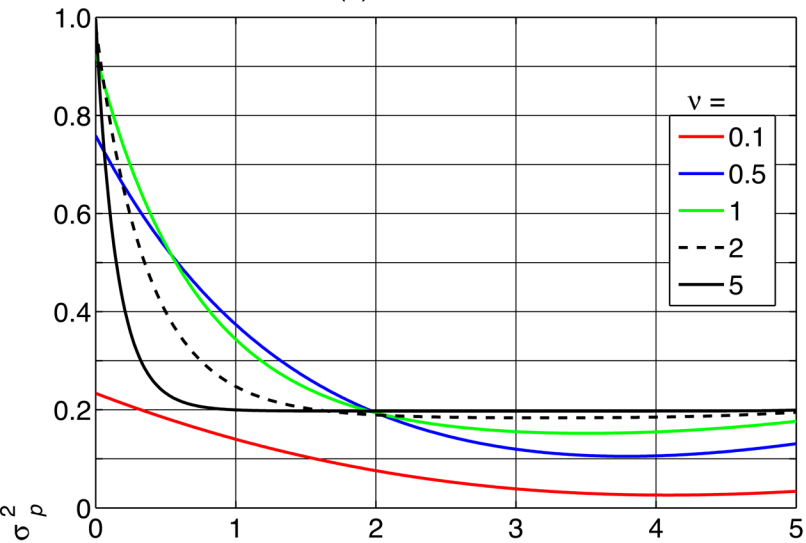
(a) Theory



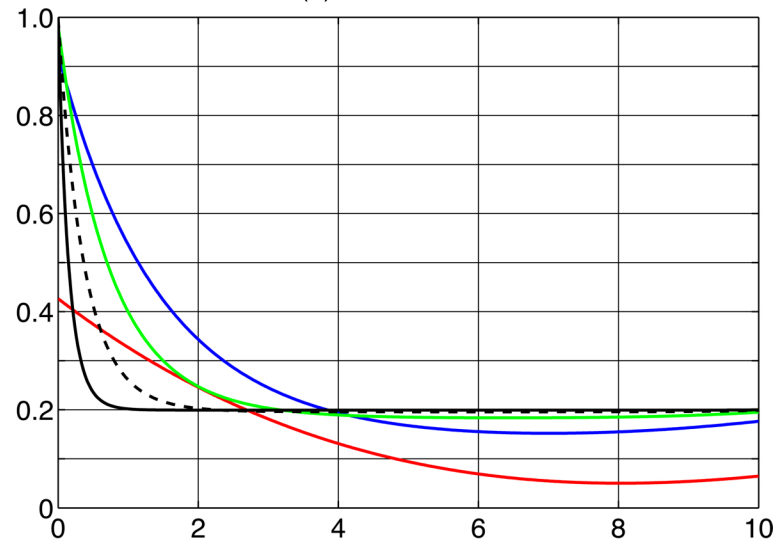
(b) FS



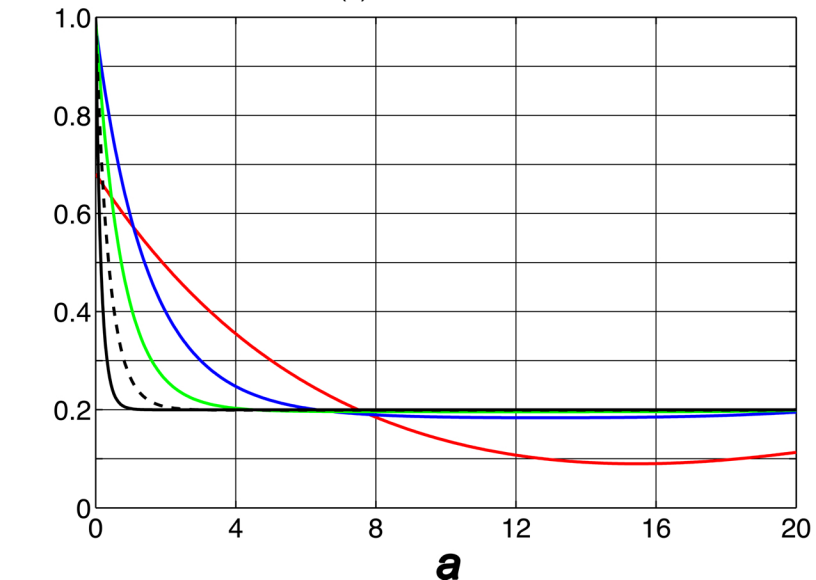
(a) Area = 10 x 10



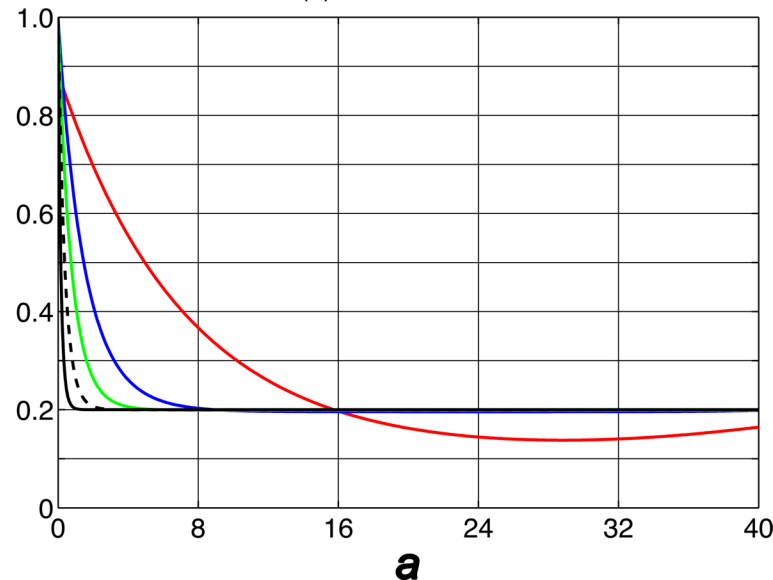
(b) Area = 20 x 20



(c) Area = 40 x 40

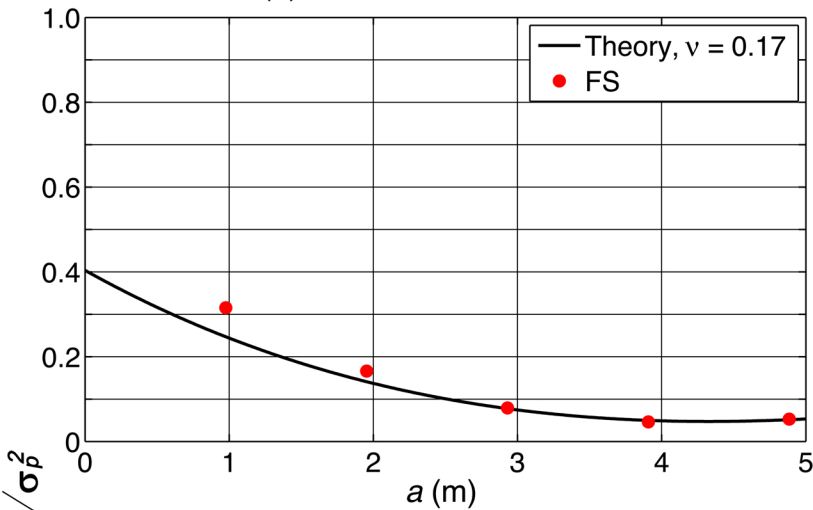


(d) Area = 80 x 80

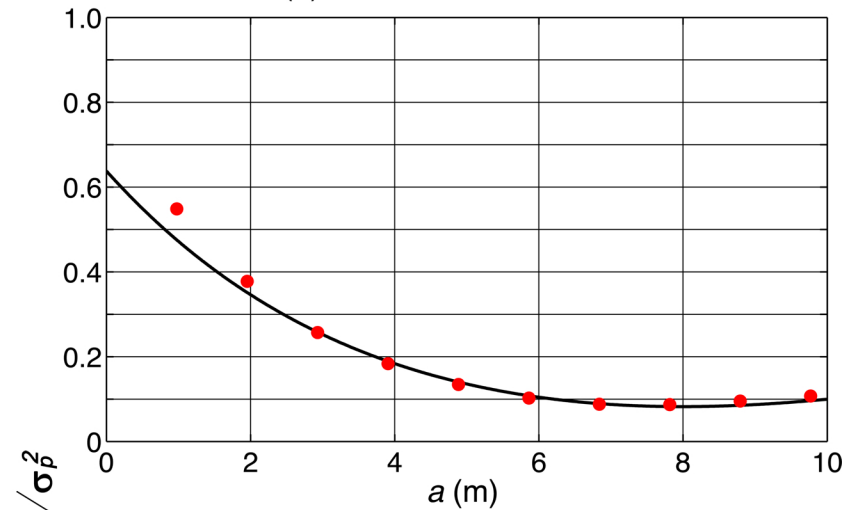




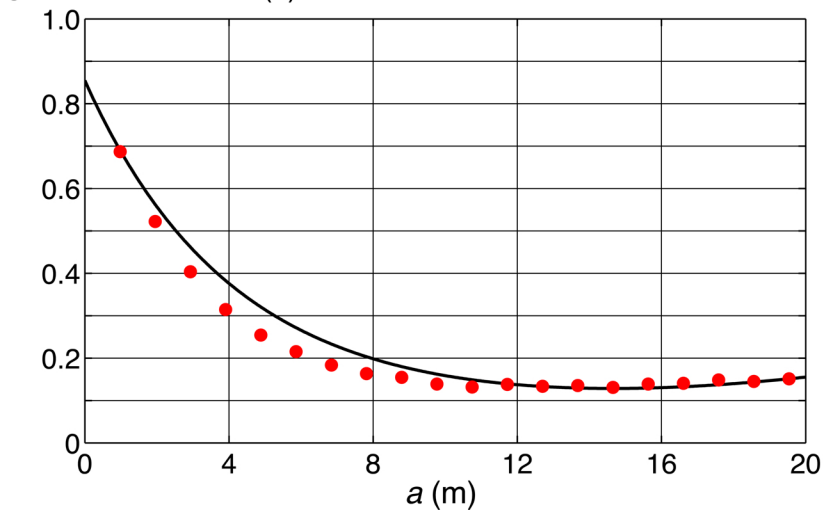
(a) Area = 10.7 m x 10.7 m



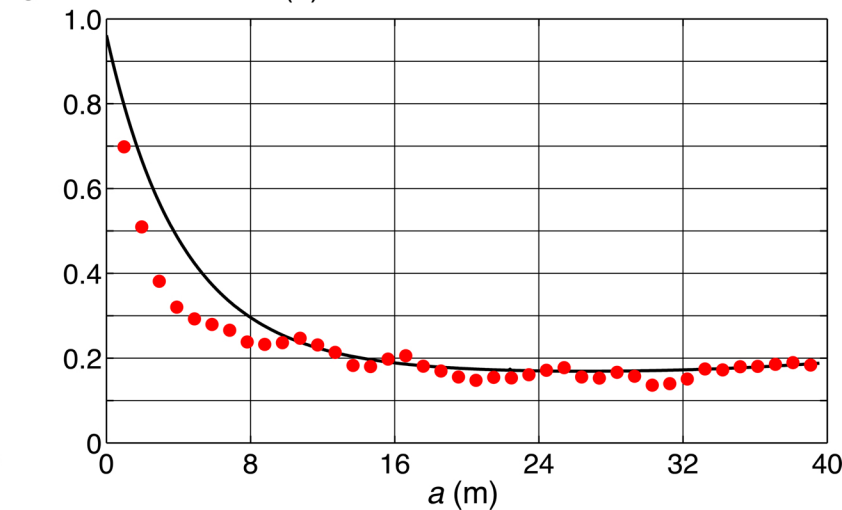
(b) Area = 20.5 m x 20.5 m



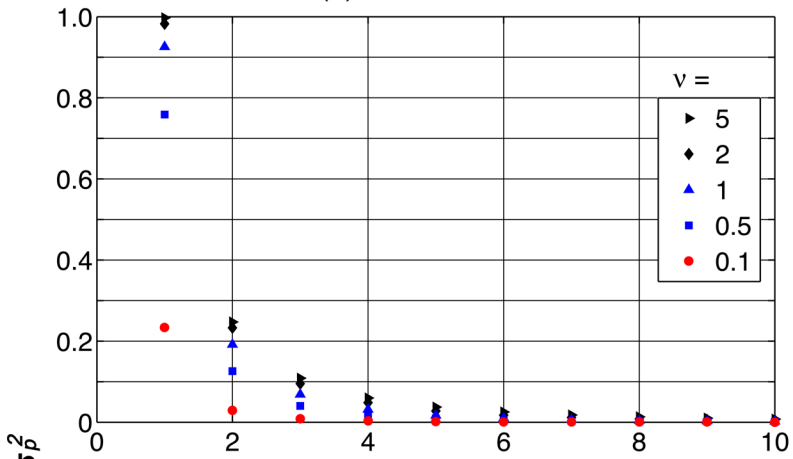
(c) Area = 40.1 m x 40.1 m



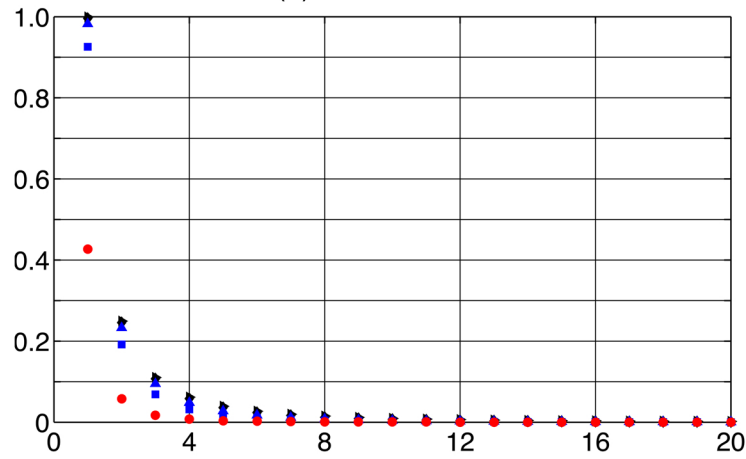
(d) Area = 79.1 m x 79.1 m



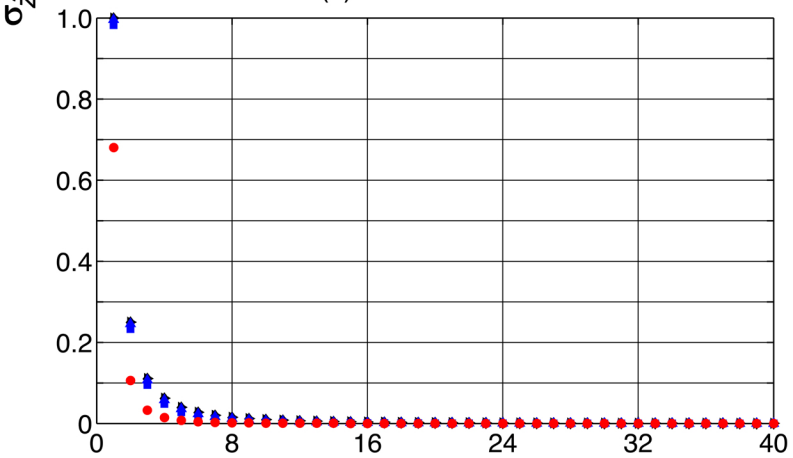
(a) Area = 10 x 10



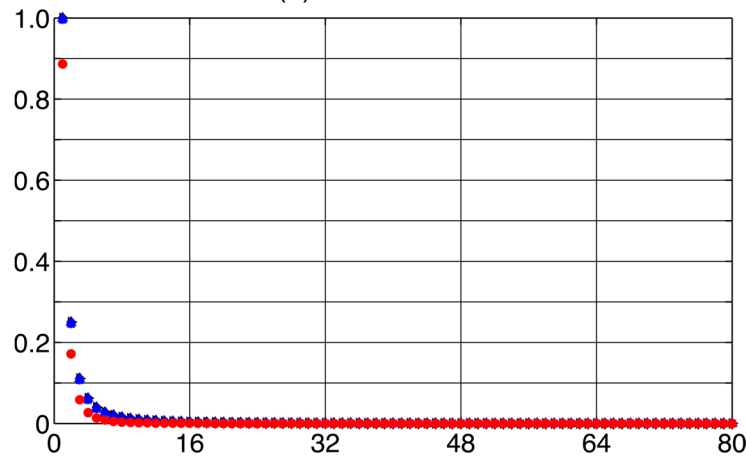
(b) Area = 20 x 20



(c) Area = 40 x 40

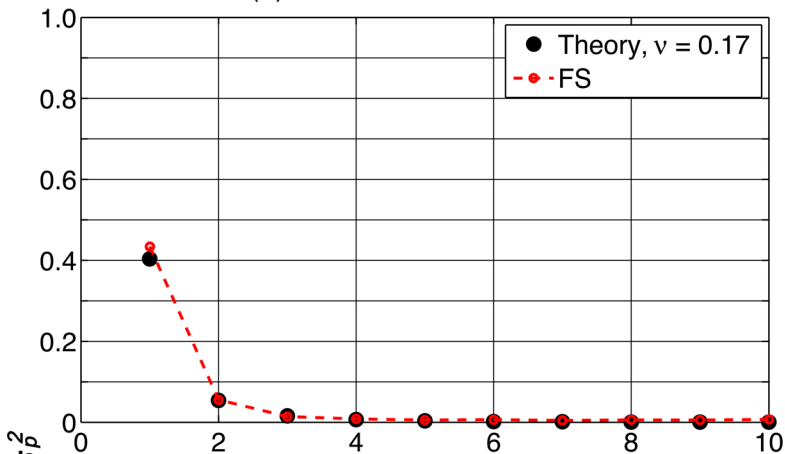


(d) Area = 80 x 80

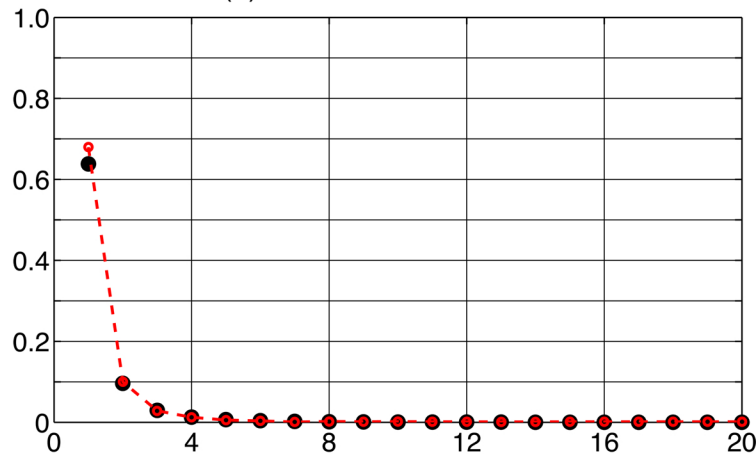


**Number of Point Measurements per side**

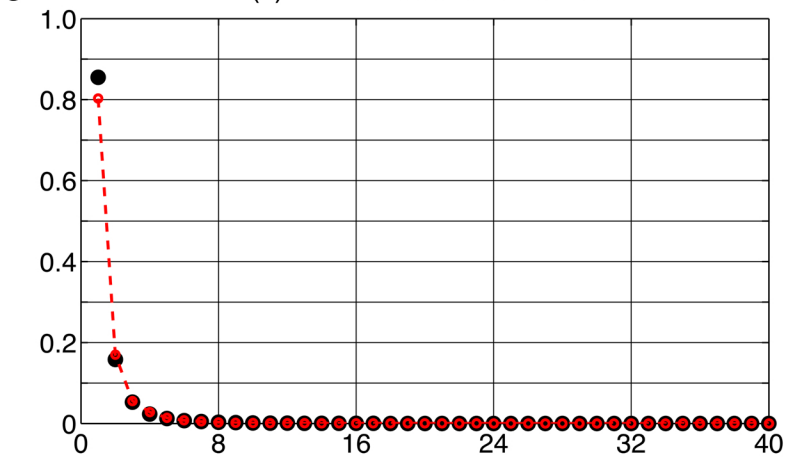
(a) Area = 10.7 m x 10.7 m



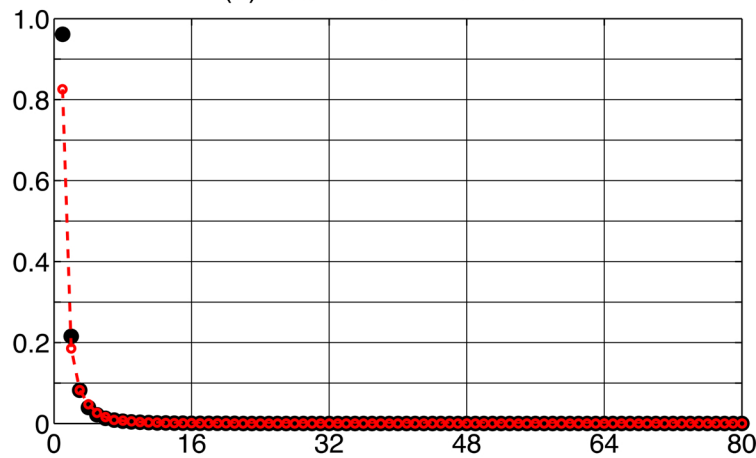
(b) Area = 20.5 m x 20.5 m



(c) Area = 40.1 m x 40.1 m



(d) Area = 79.1 m x 79.1 m



Number of Point Measurements per side